MASTER

Assessing hypoxic ischemia in the neonatal brain
accuracy of diffusion weighted imaging in MR

van den Tillaart, J.R.M.

Award date:
2004

Link to publication

Assessing hypoxic ischemia in the neonatal brain
*Accuracy of Diffusion Weighted Imaging
in MR*

Afstudeerverslag
Jannie van den Tillaart

FIK/KFM   2002-01

Technische Universiteit Eindhoven
Faculteit Technische Natuurkunde
Capaciteitsgroep Fysische Informatica en Klinische Fysica

Eindhoven, februari 2002
Afstudeerverslag
Docent: prof.dr.ir. P.F.F.Wijn
Begeleider: ir. C. van Pul

Summary

A new MRI-technique is called Diffusion Weighted Imaging (DWI). On a DW image the contrast is determined by the way the water molecules are able to move, diffuse, through the tissue. With this technique abnormalities can be detected earlier than with the conventional techniques, because tissues in distress often show a changed diffusion while the tissue structure is still intact.

The average displacement of the water molecules in a volume unit can also be visualized and expressed as a value, called the Apparent Diffusion Coefficient (ADC). The ADC is proportional to the amount of diffusion: a decrease of diffusion results in a decrease of the ADC.

In this study it is examined whether the ADC can be used for the early detection of hypoxic ischemia and whether the ADC can be used to classify the phase of an infarct caused by hypoxic ischemia and for the classification of brain development.

The inter human variation of the ADC for different brain tissues is determined for healthy volunteers and is relatively small (5-8%). Because the inter human variation is small the ADC can possibly be used to measure brain development. The decrease in the ADC for ischemic tissue compared to healthy tissue is large enough (40-50%) to make a distinction between them. This makes the ADC useful for the early detection of hypoxic ischemia.

Unfortunately, the ADC depends on several parameters like the number of b-values used and on which b-values are used. Whether the ADC is accurate enough to be used quantitatively is examined in more detail.

For this purpose factors that influence the ADC are discussed. For two of these factors, the background imaging gradients and the bias caused by noise, correction methods are given. Measurements are performed on a water phantom, an orange and a volunteer to investigate what happens to the ADC when different parameters of the PFG's are changed.

From the results of these measurements it can be concluded that the ADC depends on the parameters that are used. The two correction methods are applied, but neither of them improves the results significantly.

The final conclusion is that ADC's can only be compared quantitatively if they are measured on the same clinical scanner using the same parameters.

It is recommended to use the same protocol for all the DWI measurements.

Due to new software on the scanner it should be checked if the normal values presented in this study can be used for comparison.

Assessing hypoxic ischemia in the neonatal brain
Accuracy of Diffusion Weighted Imaging in MR

Contents

Summary

Chapter 1
Diffusion Weighted Imaging in the neonatal brain.

§1.1 Introduction

Magnetic Resonance Imaging (MRI)

Magnetic Resonance Imaging is a diagnostic technique that can be used to make high-resolution images of the human body without using radiation. For diagnosis of brain damage in neonates, MRI is preferred to the CT (Computed-Tomography), which does use radiation. The MRI-technique is based on the magnetic behavior of the water molecules; the human body consists of about 60-80% water. When the water molecules are placed in a strong magnetic field their equilibrium can be disturbed, generating a signal that can be measured. The time it takes to reach equilibrium again depends on the way the equilibrium was disturbed and on the structure of the tissue.
Each tissue has it own characteristic relaxation times (called T1 and T2). On a conventional MR image the contrast is determined by the relaxation times and thus by the structure of the tissue, the images are called T1- are T2-weighted images.

Diffusion Weighted Imaging (DWI)

A new MRI-technique is called Diffusion Weighted Imaging. On a DW image the contrast is determined by the way the water molecules are able to move, diffuse, through the tissue. With this technique abnormalities can be detected earlier than with the conventional techniques, because tissues in distress often show a changed diffusion while the tissue structure is still intact.

An important application of DWI is the detection of hypoxic ischemia by premature newborns. Hypoxic ischemia is a lack of oxygen in the brain (mostly due to an infarct) and causes brain damage, which can result in seizures and spasticity.

To understand what happens by hypoxic ischemia and to understand the DWI technique better, some background information is discussed first. The aim and setup of this study is discussed second.

§1.2 Diffusion

Information about diffusion in a tissue is important for two reasons. First, diffusion is the process through which the nutrients and oxygen from the capillary vessels come into the cells. A change in diffusion is an indication for problems with the nutrient supply to the cells. Visualizing this change in diffusion helps to detect tissue in distress earlier, making treatments more effective. Second, the preferred direction of the diffusing water molecules contains information about the tissue structure.

Diffusion in healthy tissue

Water molecules move constantly, due to Brownian motion. The velocity of the movement depends on the environment and temperature. When the environment contains only other water molecules, the movement is only restricted by the bouncing of the molecules against one another, this is called free-diffusion.

In a tissue, the molecules interact also with cell membranes, cell parts and other macromolecules, as shown in Figure 1.1b, this is called restricted diffusion. When the diffusion is restricted in the same way in all directions, it is called isotropic (restricted) diffusion. When the diffusion is restricted more in one direction than in the other direction, it is called anisotropic (restricted) diffusion, as shown in Figure 1.1c. The water molecules have a preferred direction in which they move.
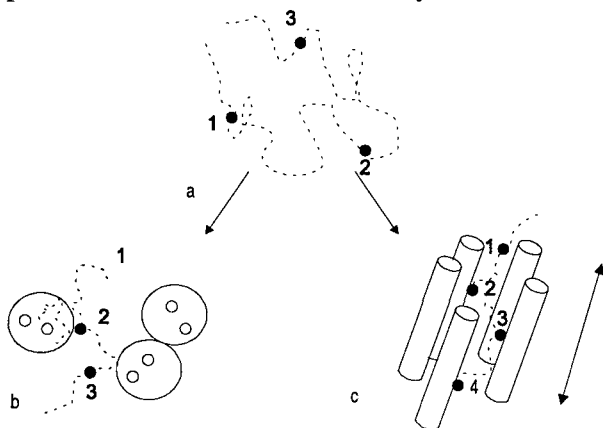
Figure 1.1: Diffusion of water molecules a) the diffusion is only restricted by the other water molecules. b) the diffusion is influenced by the cell membrane. c) the diffusion is restricted by the myelin sheaths around the fibers, the arrow indicates that the preference direction of the diffusion lies along the fiber orientation.

Diffusion in ischemic tissue

In ischemic tissue, the oxygen supply to the cells is disturbed, resulting in an uncontrolled water transport through the cell membrane. The cell starts to swell and the diffusion of the water molecules decreases. The underlying processes that cause the decrease in the diffusion are not precisely known. A possible explanation is that the movement of the water molecules is more restricted due to the cell swelling. They cannot move around the cells as easy as they could before the swelling, as illustrated in Figure 1.2b.

2

Figure 1.2: a) Diffusion before the cells are swelling. b) The decrease of the diffusion is possibly caused by the extra restriction of the movement of the water molecules due to cell swelling.

When no treatment is given the cells will eventually loose their function, resulting in brain damage.

DWI by hypoxic ischemia

The difference between conventional MR and DWI lies in an extra component, the Pulsed Field Gradients (PFG's), that make the measurement sensi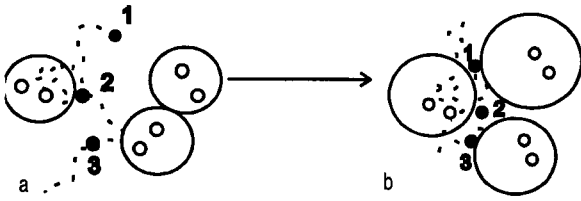tive for diffusion. The diffusion causes a decrease of the signal. The lower the diffusion, the higher the signal, resulting in a lighter pixel on the image. With DWI, the diffusion of water molecules is measured in three directions. The average of these three images results in an image in which the diffusion is displayed independent of the direction, called an isotropic image. When the measurements are performed in six directions, the preferred diffusion direction of the water molecules can be visualized, this is called Diffusion Tensor Imaging (DTI).
When the diffusion is decreased as in hypoxic ischemia, the signal is less attenuated and the pixel becomes lighter. Areas that are affected by hypoxic ischemia appear brighter on the DWI, in this way the ischemic tissue can be visualized in an early stage.

The average displacement of the water molecules in a volume unit can also be visualized and expressed as a value, called the Apparent Diffusion Coefficient (ADC). The ADC is proportional to the amount of diffusion: a decrease of diffusion results in a decrease of the ADC.

As mentioned above, the diffusion of ischemic tissue changes. Different phases in the change of diffusion can be distinguished, as shown in Figure 1.3.
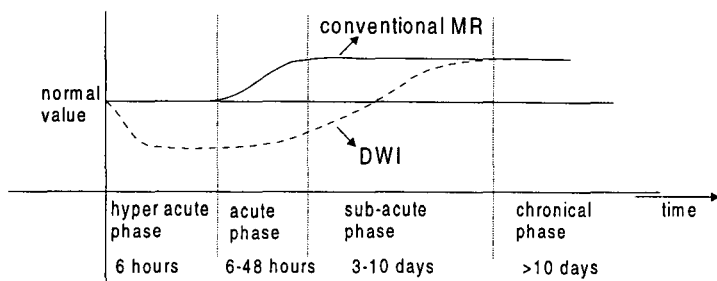
Figure 1.3: The different phases that can be distinguished after an infarct, on DWI and conventional MRI.

In the hyper acute phase, the ADC is lower in the area that is affected by ischemia than in healthy tissue. The T2 image made with conventional MR is unchanged.
In the acute phase, the ADC is still lower than for healthy tissue and the T2 value is higher.
In the sub-acute phase, the ADC is in the beginning lower than the healthy tissue, and gradually the ADC becomes larger than the healthy tissue. The T2 value is still higher.
In the chronical phase, both the ADC and T2 value are higher than for healthy tissue.

Depending on the phase of the infarct, the infarct can be visualized using DWI, conventional MR technique or both. By combining the conventional MR techniques and DWI an estimation can be made how long ago the infarct occurred.

Summarizing:
- A DW image can be used for the detection of the infarct in an early stage, before irreversible brain damage.
- By combining DWI and conventional MR techniques an estimation can be made on how long ago the infarct occurred.

Figure 1.4 and 1.5 show examples of conventional MR images together with the DWI and ADC images.

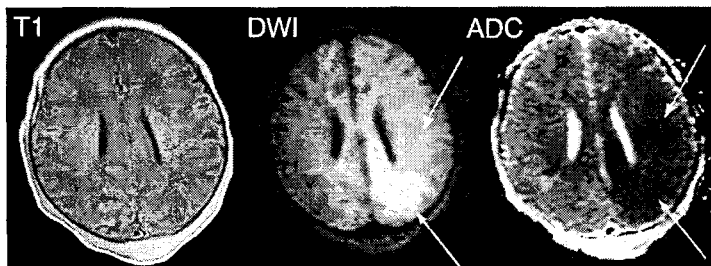*Figure 1.4:The brain of a neonate suffering from hypoxic ischemia. On the conventional MR image the infarct due to hypoxic ischemia cannot been seen. On the DWI the infarct appears brighter and on the ADC image it appears darker.*
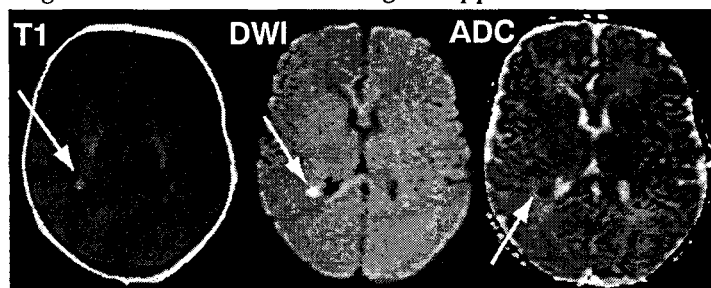

Figure 1.5: The brain of a neonate suffering from hypoxic ischemia. Only a small area is affected by the infarct; the infarct is older and is visible on the DWI and conventional image.

4

§1.3 Aim of the study

The Saint Joseph Hospital in Veldhoven is one of the ten hospitals in the Netherlands that has a Neonatal Intensive Care Unit (NICU). This unit is specialized in taking care of critically ill newborns. About 75% of these newborns are born prematurely, a large group of these newborns suffer from hypoxic ischemia.

Together with the NICU we want to investigate whether DWI can be used for early detection of the hypoxic ischemia and whether the ADC can be used quantitatively to classify the phase of the infarct and the brain development

The problem with the early detection of the infarct is that newborns suffering from hypoxic ischemia are usually too unstable to undergo a MRI scan and the MRI scanner is not always available. Therefore, most scans are made in a later stadium and the infarct can be visualized using conventional MRI techniques and the ADC image is used to provide information about the moment that the infarct occurred.

It is also important to know how the brain develops. When the brain develops, the tissue structure changes causing a change in the preferred diffusion direction of the water molecules, this can be visualized using DTI. DTI is therefore discussed briefly in this report to evaluate its possibilities.

§1.4 Structure of the report

To understand DWI and DTI some background information is necessary; therefore the basics of Magnetic Resonance Imaging are discussed in the next chapter. This chapter is followed by a chapter in which the theory of Diffusion Weighted Imaging is explained.

When the ADC is used to obtain information about the infarct it is important to have a reference ADC. Therefore the inter-human variation is determined for healthy volunteers, healthy newborns and for newborns suffering from hypoxic ischemia. The normal values are given in chapter 4. Problems that occurred by determining these normal values are discussed.

To examine whether the ADC values found in chapter 4 can be used quantitatively, information is needed about the system factors that influence the ADC. A summation of system factors and the errors they can cause is given in chapter 5.

From two of these system factors it is known from literate that they can lead to large errors, especially when the so-called EPI-sequence is used for DWI. The EPI-sequence is used because the scan-time should be as short as possible for the patients' comfort. The two system factors and possible correction methods are treated in more detail in chapter 6.

To check whether the ADC can be used quantitatively, different measurements are performed. The measurements and their results are discussed in chapter 7. The correction methods described in chapter 6 are tested and their results are also given in chapter 7.

In the last chapter, chapters 8, conclusions and recommendations are given.

Chapter 2
Basics of Magnetic Resonance Imaging.

The concept of Magnetic Resonance Imaging (MRI) is based on the interaction between the spins of protons and a magnetic field. The behavior of spins in a magnetic field is described in the first paragraph. In the second paragraph it is explained how this effect can be used to create an image, using a Spin Echo (SE) sequence as an example. In the third paragraph, another type of sequence and k-space are discussed. In the fourth paragraph the building blocks of a MRI scanner are discussed.
This chapter is mainly based on [1], [2], [3] and [4].

§2.1 Magnetic Resonance Imaging

The human body consists of about 60-80% water, which itself consists of oxygen and two protons with spin ½. The rotation axis of the magnetic moments (μ) of the protons will align parallel or anti-parallel to the direction of an applied magnetic field. The magnetic moments can have another direction than the main magnetic field, causing them to precess around the direction of the main magnetic field, with the Larmor frequency, as shown in Figure 2.1a. The Larmor frequency is given by:

$$\omega_0 = \gamma |B_0|$$
(2.1.1)

with γ = gyromagnetic ratio
         ω_0 = Larmor frequency
and B_0 = the main magnetic field

The magnetic moments add up to a net magnetization vector along the direction of the applied magnetic field, Figure 2.1c.

A rotating frame of reference is introduced. In this coordinate system the z'-axis is parallel to B_0 and the x'- and y'-axes rotate around the z-axis with the Larmor frequency, Figure 2.1b. In the rotating frame of reference the magnetic moments stand still and there appears to be no active magnetic field.
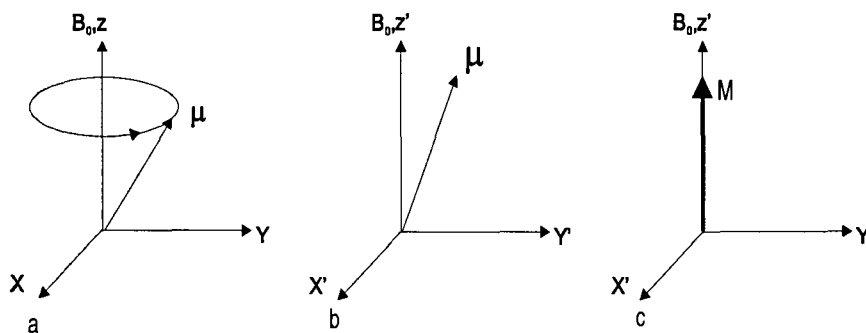

Figure 2.1: a) Precession of the magnetic moment around the main magnetic field in the laboratory frame. b) The magnetic moments stand still in the rotating frame of reference c) In the rotating frame of reference the magnetic moments add up to a net magnetization vector (M) parallel to z'.

An extra magnetic field B_1 will be applied in the rotating frame, causing the magnetization vector to precess towards the x'y'-plane. The time that B_1 is applied determines the flip angle of the vector with respect to the z'-axis, as shown in Figure 2.2a. The flip angle can be calculated by:

$$\alpha = \gamma B_1 \tau \tag{2.1.2}$$

with α = flip angle
and τ = duration of B_1

Usually a RF pulse is applied that rotates the magnetization vector completely into the x'y'-plane in a time t=t_{90}, the flip angle is 90°, as shown in Figure 2.2a.
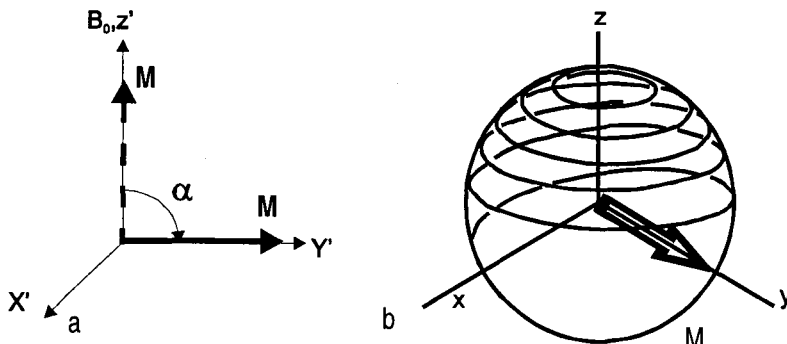
Figure 2.2: a) The flip angle of the net magnetization vector b) Precession of the net magnetization to the xy-plane viewed in the laboratory frame

The magnetic field B_1 stands still in the rotating frame of reference, but rotates with the Larmor frequency ω_0 in the laboratory frame.
The magnetization vector, described by the Bloch equations, relaxes back to equilibrium in a characteristic time depending on tissue properties.

Directly after excitation, when B_1 has become zero again, all spins precess with the same phase around the z'-axis and the net magnetization vector in the x'y'-plane has a maximum signal. The signal decays exponentially due to two effects. The first effect is caused by the spin-lattice relaxation, resulting in a change of the longitudinal component of the net magnetization vector (T_1-decay). The second effect is caused by the spin-spin relaxation, resulting in a change of the transverse component of the magnetization vector (T_2-decay). The T_2-decay is also influenced by field inhomogeneities resulting in T_2^*-decay, this decay can be calculated through

$$\frac{1}{T_2^*} = \frac{1}{T_2} + \frac{1}{T_{2,inhomogeneties}} \tag{2.1.3}$$

The changes of the magnetic vector can be measured with a current loop; only the change in the transverse component is measured.

Eventually the current through the current loop will die out due to the T_1 and T_2 effects. The signal measured is called the free induction decay (*FID*), Figure 2.3.
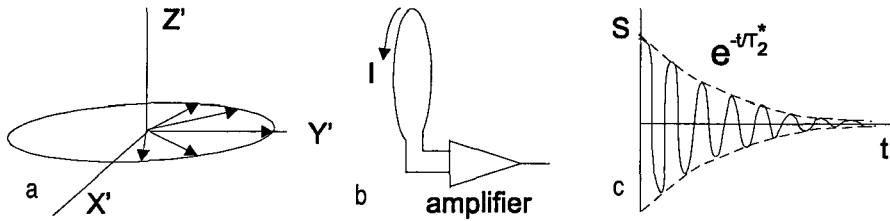
Figure 2.3: a) The dephasing of the spins due to T_2^* relaxation. b) A current loop is used to measure the change of the transverse component. c) The measured signal decays exponentially and is called free induction decay.

§2.2 Imaging

As described above, all spins are excited independent of their position in the body. To make an image it is necessary to measure the signal as a function of position in the body. In this paragraph it is explained how a slice can be selected and how the signal as a function of position can be determined, using a spin echo (SE) sequence as an example. The main magnetic field is defined along the z-axis, the measurement direction is defined along x-axis and the phase-encoding direction is defined along the y-axis.

The SE sequence is the most fundamental sequence in MRI. A sequence can be shown as a time diagram, which determines which gradients are turned on and the moment that they are turned on. The SE sequence is given in Figure 2.4.
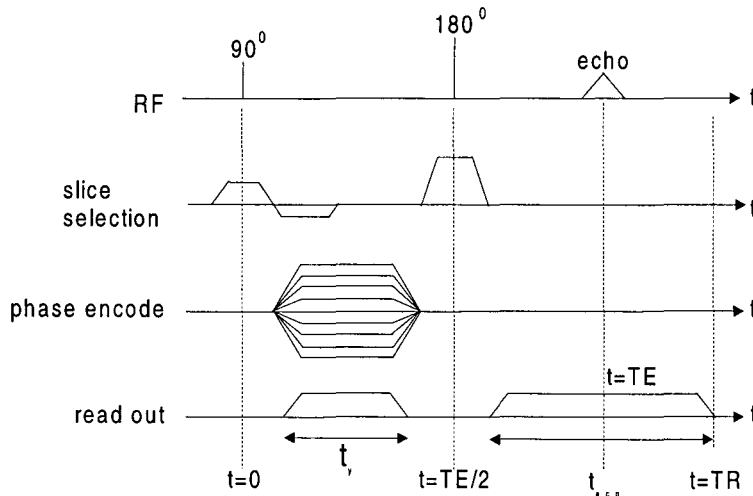
Figure 2.4: The SE sequence. In this time diagram it can be seen which gradients are turned on and when they are turned on. The G_z is the slice selection gradient, G_y the phase encoding direction and G_x is the read-out direction.

The way an image is made is explained using the SE sequence as an example, the sequence will be explained step by step.
The first gradient as shown in Figure 2.4 is a slice-selecting gradient in the z-direction.

Slice selection

In equation (2.1.1) is shown that the precession frequency of the magnetic moments depends on the applied magnetic field. By superimposing a linear magnetic field on top of the main magnetic field, the precession frequency becomes a function of position. The linear magnetic field is described by:

$$\frac{dB}{dz} = G_z z \qquad (2.2.1)$$

with dB/dz = the gradient field in the z-direction
               G_z = strength of the gradient field
and z = the direction of the applied gradient field

The total magnetic field becomes

$$B_{tot} = B_0 + G_z \cdot z \qquad (2.2.2)$$

The frequency of the magnetic moments depends on their position in the z-direction (Figure 2.5a). A slice between z_1 en z_2 can be selected by using frequencies between f_1 and f_2, (Figure 2.5b). To obtain a rectangular RF pulse, a sinc-function has to be given in the time domain (Figure 2.5c).

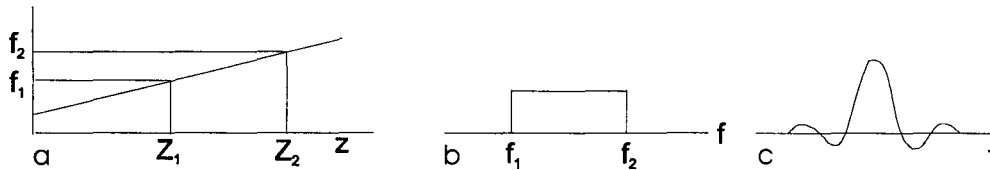*Figure 2.5: a) Slice selection with a gradient field, the frequency band is shown. b) The frequency spectrum of the RF pulse. c) The RF pulse in the time domain.*

With the first gradient in the time diagram of Figure 2.4 a slice is selected. The other two gradients that are turned on in Figure 2.4 are gradients that determine the position of the signal within the slice: the read-out gradient and a phase-encoding gradient.

The read-out gradient

By applying a gradient in the x-direction during the time that the signal is measured the position of the magnetic moments in the x-direction can be encoded, because the rotation frequency of the magnetic moments depends on their x-position, Figure 2.6. From the received signal, containing information from all positions, the original frequencies and their amplitude can be obtained by Fourier Analysis. The frequency characterizes the position of the spins in the x-direction (read-out). The amplitude is proportional to the magnitude of the magnetization at this position.
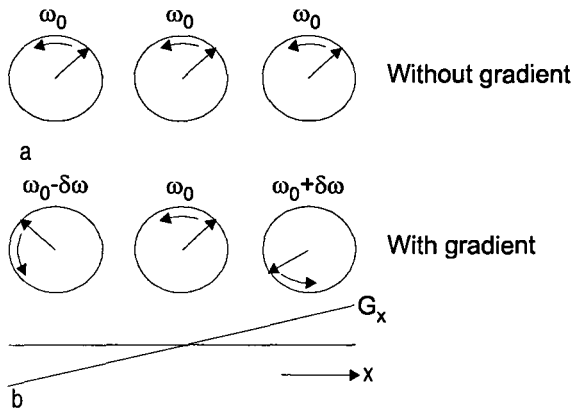
Figure 2.6: a) When no read-out gradient is on, the spins will precess with the same frequency ω_0, as shown for three positions. b) When the read-out gradient (G_x) is turned on, the spins will precess with different frequencies, depending on their positions.

The phase encoding gradient

To make an image, the position in the y-direction (called phase encoding direction) should also be known. By applying a gradient in the phase encoding direction during a short time, the spins will rotate with different frequencies for a short period of time, and thus their phase will be changed, Figure 2.7. By measuring the change in the phase of the spins, the position in the y-direction can be determined.
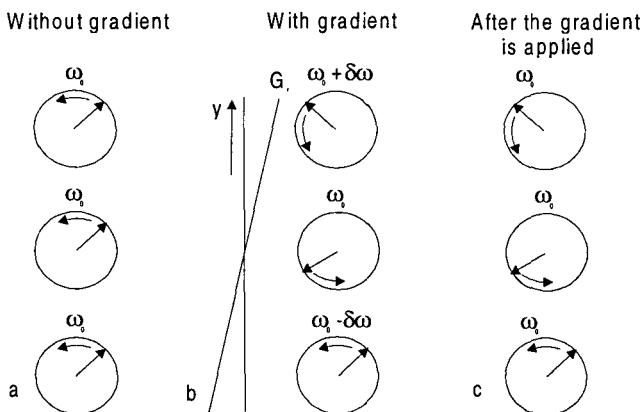
Figure 2.7: a) When no phase-encoding gradient is on, the spins will precess with the same frequency ω_0, as shown for three positions. b) When the phase-encoding gradient (Gy) is turned on, the spins will precess with different frequencies depending on their positions. c) When the phase-encoding gradient is turned off, the spins will precess with the same frequency again, but there is a difference in the phase.

10

To measure a phase difference between two points, two measurements are needed, when the signal is made up from N points then N measurements are needed

As shown in the time diagram, Figure 2.4, first a 90° is used, followed by a 180° pulse after a time t=TE/2. After the 90° pulse the spins will dephase due to field-inhomogeneities, this FID signal will die out. After t=TE/2 the 180° pulse will force the spins to rephase, which is complete after time TE. After which they will start to dephase again (Figure 2.8). The signal is measured after the 180° pulse, using a gradient in the read-out direction (Figure 2.4). The signal is called a spin echo (SE), Figure 2.9
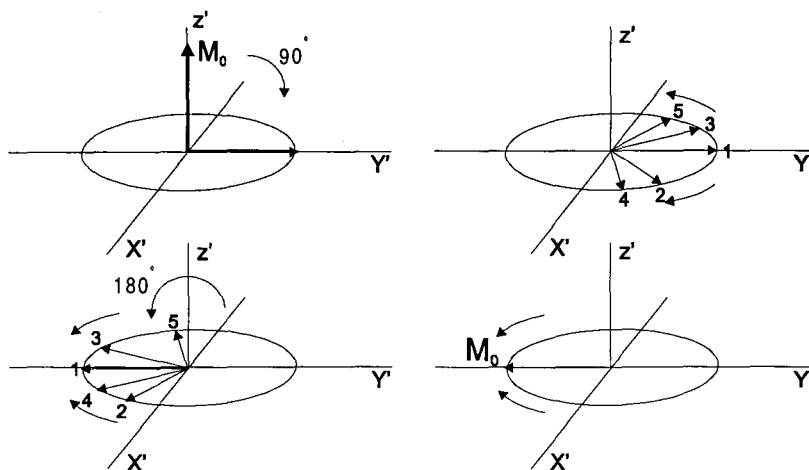
Figure 2.8: a) Excitation of the magnetization vector with a 90° pulse. b) Dephasing. c) Rotation with a 180° pulse. d) Rephasing at time t=TE all the spins align again.
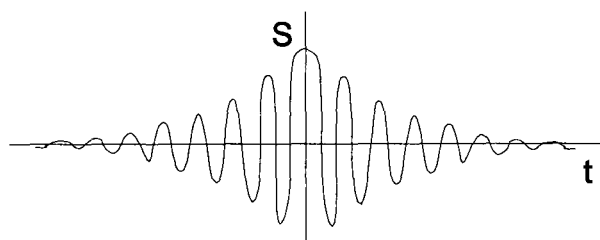
Figure 2.9: The signal, S, measured in SE

In order to make an image, first a slice is selected and within this slice the position is encoded using a readout gradient and a phase encoding gradient.

The measured signal results from the relaxation of the net magnetization vector described by the Bloch equation:

$$\frac{d\bar{M}}{dt} = \gamma(\bar{M} \times \bar{B})$$

(2.2.3)

The Bloch equation for the longitudinal (z') and transversal (T) direction becomes:

$$\frac{dM_T}{dt} = (\omega_0 - \omega)M_{y'} - \frac{M_{x'}}{T_2}$$

(2.2.4)

$$\frac{dM_{z'}}{dt} = -\frac{(M_z - M_{z0})}{T_1}$$

In the preceding section magnetic resonance imaging is discussed using the SE sequence as an example, but there are other faster imaging techniques. Differences between sequences are best explained using k-space. Therefore k-space is explained in the next paragraph for the SE sequence and next the differences between the SE sequence and the EPI sequence are discussed.

§2.3 Sequences and the k-space

The signal is measured in the time domain, but information about the spin positions is obtained in the frequency domain. From the signal, the original frequency and amplitude of the spins can be obtained by the Fourier transformation. The k-space is defined by the phase encoding and read-out steps, x and y are transformed to k_x and k_y through

$$k_i = \gamma G_i t' = \gamma \int_0^{t'} G_i(t)dt \qquad i = x, y$$

(2.3.1)

Notice that k_x and k_y have dimension m^{-1}.

The measurement must be performed in such a way that k-space is filled to reconstruct the image. First, the k-space is discussed for the SE sequence later k-space is discussed for the EPI sequence.

The k-space

The trajectory of the SE sequence through the k_x,k_y-plane is given in Figure 2.10.
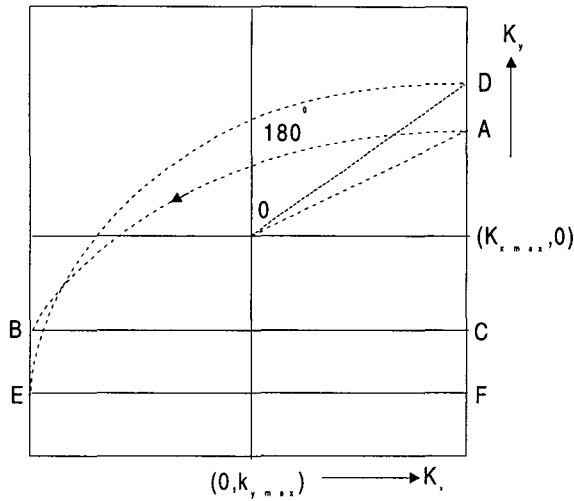
Figure 2.10: Trajectory of the Se-sequence in the k-space.

Between t=0 and t=TE/2 both the k_x and k_y increase linearly (as can be seen in Figure 2.4, G_x and G_y are both on at the same time) and k moves from 0 to point A. The 180° pulse inverts the sign of the phase so both k_x and k_y change sign from point A to point B. Then the readout gradient is turned on and a line with constant k_y is measured. From point B to C the data is acquired. The spin system now relaxes back to equilibrium after which the process is repeated, but with a different phase encoding gradient so another horizontal line is acquired (DEF). This is repeated until the whole k-space is filled.

The number of points measured to obtain the line (BC or EF) determines the Field Of View (FOV),

$$FOV = \frac{2\pi}{\gamma G_x t_s} \qquad (2.3.2)$$

with t_s the time between two points.

The FOV determines the resolution (R) by:

$$R = \frac{FOV}{N} \qquad (2.3.3)$$

with N number of points per line.

Besides the SE sequence there are other sequences, which fill the k-space in a different way in order to decrease scan time.

The EPI sequence

The EPI sequence fills the k-space in another way than the SE sequence. In Figure 2.11 the time diagram of the EPI sequence is given. The difference between the SE sequence (Figure 2.5) and the EPI sequence can be found in the way the read-out and the phase encoding gradients are given. Smaller phase encoding gradients are given just before the readout gradients are turned on, resulting in a phase encoding gradient train and a read out train.
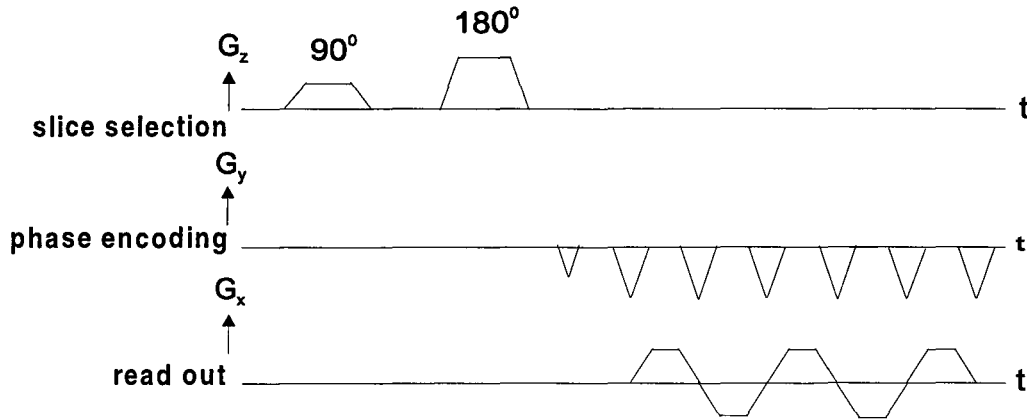
Figure 2.11: The EPI sequence.

The trajectory through k-space is given in, Figure 2.12.
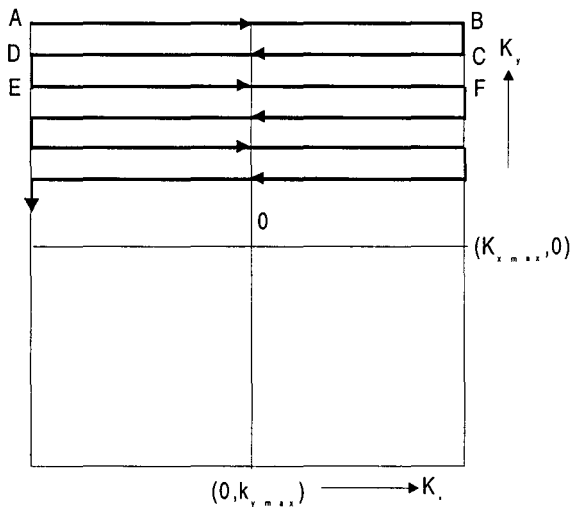
Figure 2.12: The k-space of the EPI sequence.

The first phase encoding and readout gradient position the starting point of the k-space in point A. Then a read-out gradient is applied (B) followed by the second phase encoding gradient, point C is reached. The next read-out gradient is negative, the line CD is measured. This repeats itself until all lines in the k-space are filled.

K-space can be filled in one repetition time using EPI, by the SE sequence only one line in k-space is filled during one repetition time. Notice that the magnetization vector is only once excited to the x'y'-plane for the EPI sequence (for the SE sequence this is done for each line in k-space) therefore the Signal-to-Noise-Ratio for EPI is lower than for the SE sequence.

§2.4 The MRI scanner

In the first three paragraphs the principle of magnetic resonance is discussed and the reconstruction of an image is described. In this paragraph the building blocks of a MRI scanner are discussed.

A MRI scanner is built up by the following components, Figure 2.13:
- A magnet (in clinical systems a 1.0 or 1.5 Tesla magnet) to provide the main magnetic field B_0. This field is constantly on.
- Gradient coils that provide the slice selecting, phase encoding and readout gradient
- RF coil for generating of the RF signal. The signal is measured by a coil that can be placed around the region of interest, Figure 2.15
- A patient table
- An RF shield that shields the RF fields
- A computer controls the gradient coils and the RF coil (via the Gradient pulse program, the gradient amplifier, the RF source, the Pulse Program, the digitizer, the RF detector and the RF amplifier).
- A computer screen on which the images can be displayed
- A possibility to make a film of the images

Figure 2.13: The MRI system; the magnet, the gradient coils and the RF coils have a cylindrical shape.

An example of a MRI scanner is given in Figure 2.14.

15
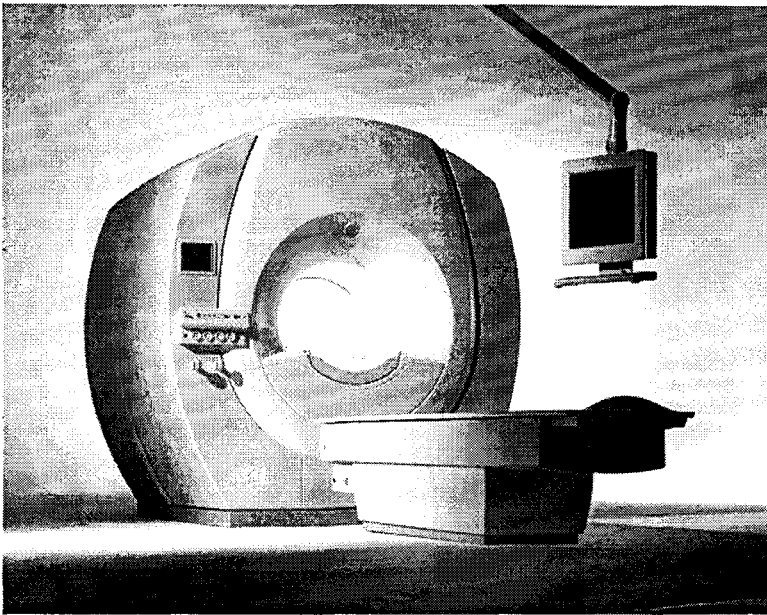
Figure 2.14: An example of an MRI scanner.

A surface coil, placed around a region of interest, measures the signal, an example of a head-coil is given in, Figure 2.15.
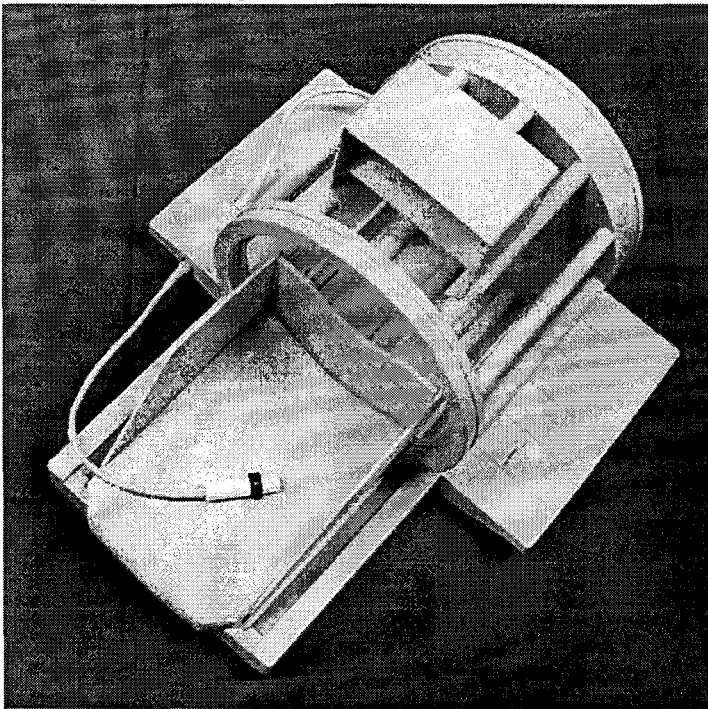
Figure 2.15: A head-coil.
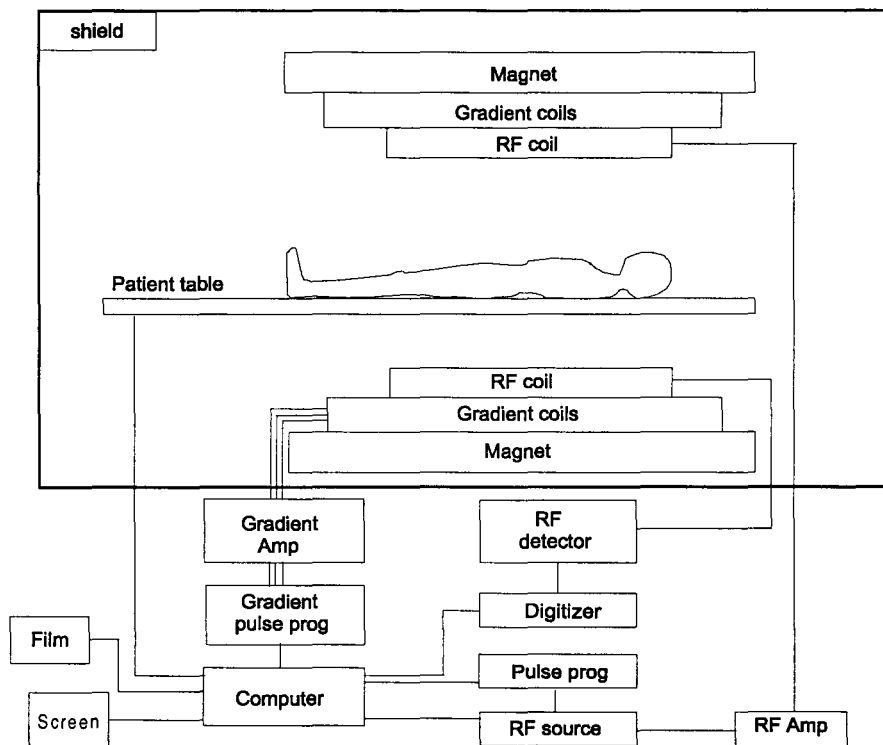
Chapter 3
Diffusion Weighted Imaging and Diffusion Tensor Imaging.

In the previous chapter the basics of MRI are given. In this chapter a new technique, called Diffusion Weighted Imaging (DWI) is discussed. DWI uses Pulsed Field Gradients (PFG's) to make the measurement sensitive for the motion of the water molecules. Stejskal and Tanner first introduced the PFG's [6]; their effect on spins and the signal is discussed in the first paragraph. From measurements with PFG's the Apparent Diffusion Coefficient (ADC) can be obtained. The aim of this study is check whether the ADC can be used quantitatively, therefore the way that the ADC can be obtained with DWI is discussed in more detail in the second paragraph. When the measurement directions are expanded from three to six the tissue structure can be visualized (DTI). DTI is discussed in the third paragraph.

§3.1 Diffusion Weighted Imaging

A large part of the human body consists of water molecules. These molecules experience two sorts of microscopical motion namely random motion (diffusion or Brownian motion) and motion caused by flow. The PFG's have a different effect on static (not moving), moving and diffusing spins, which makes it able to distinguish them from one another. The effect of PFG's are first discussed in general and then for the static, moving and diffusing spins. The signal measured for diffusing spins is discussed in more detail.

Pulsed Field Gradients

Pulsed field gradients are gradients that are applied around the 180° refocusing pulse, as shown in Figure 3.1.
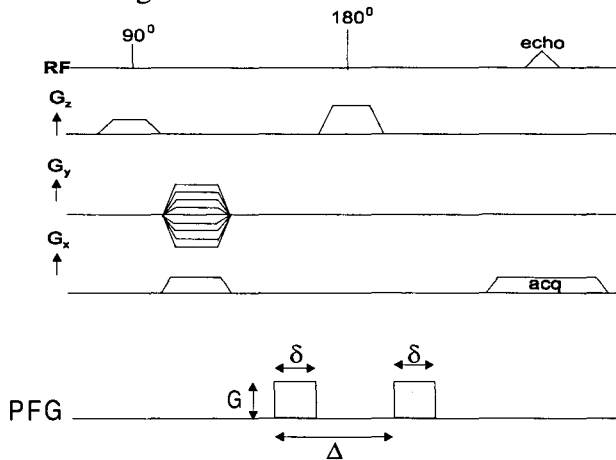
Figure 3.1: The diffusion sensitizing gradients (PFG's) around the 180° refocusing pulse.

The first PFG gradient lobe causes an extra dephasing of the magnetization resulting in a phase shift of the spins of:

$$\phi_1 = \gamma z_1 G \delta \tag{3.1.1}$$

with ϕ_1 = phase shift due to the first gradient
z_1 = Position of the spin when the first pulse is given
G = Strength of the pulse
and δ = Duration of the pulse

The second gradient pulse rephases the extra demagnetization, caused by the first pulse. The measured phase shift of the spins is now:

$$\phi_2 = \gamma z_2 G \delta \tag{3.1.2}$$

with ϕ_2 = phase shift due to the second gradient
and z_2 = position of the spin when the second pulse is given

The net phase shift that the spins experience is

$$\Delta\phi = \gamma \delta G (z_2 - z_1) \tag{3.1.3}$$

Static, moving and diffusing spins

For static spins the net phase shift, caused by the PFG's, is zero (z_2 equals z_1), the spins refocus completely and the signal intensity is decreased by the T_2-relaxation. For water molecules that move with a flow, there is a phase shift, z_1 is not equal to z_2. The signal intensity is only decreased by T_2-relaxation. For molecules that experience Brownian motion the second gradient cannot refocus the spins completely due to the diffusion. This results in a decrease of the signal intensity on top of the T_2-relaxation, while there is no net phase shift. The effects of the PFG's are illustrated in Figure 3.2.
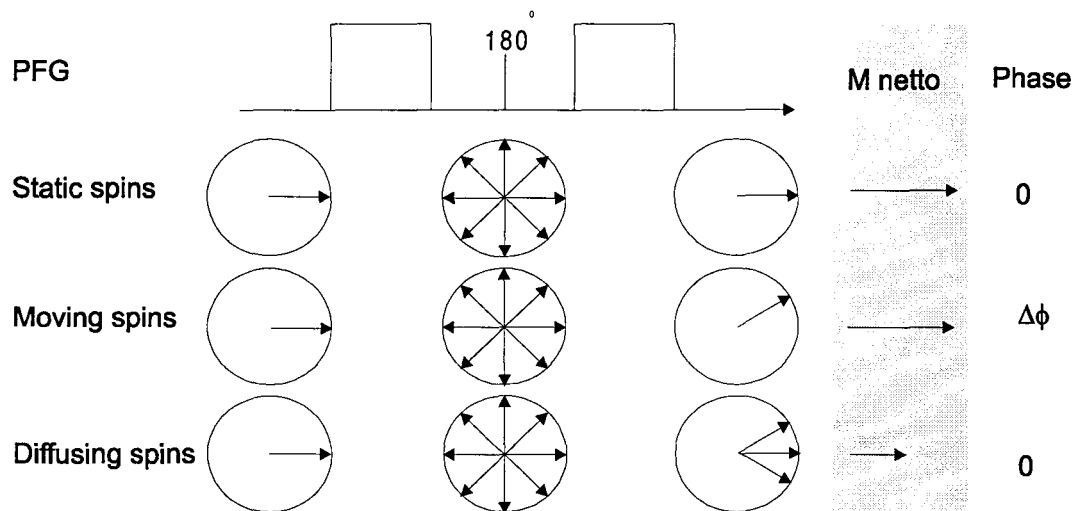
Figure 3.2: The influence of PFG on static, moving and diffusing spins.

The signal

In Figure 3.2 it can be seen that for diffusing spins the PFG's cause an extra dephasing of the spins resulting in a decrease of the signal. The measured signal thus contains T_2-decay and decay due to diffusion. The signal that is measured at t=TE can be described with the Bloch equation.

The signal measured without PFG's becomes

$$S_0 = S(0)\exp(-\frac{TE}{T_2})$$

(3.1.4)

When PFG's are applied an extra term appears in this equation, the signal becomes

$$S_b = S(0)\exp(-\frac{TE}{T_2})\exp[-bADC]$$

(3.1.5)

with
S_0 = signal measured without PFG's
S_b = signal measured with PFG's
$S(0)$ = signal at time t=0
b = the b-value (s/mm^2)
and ADC = Apparent Diffusion Coefficient (mm^2/s)

The first exponent in (3.1.5) describes the decay caused by T_2-relaxation and the second exponent describes the decay caused by the effect of the PFG's on the diffusing spins.

In order to determine the ADC from the signals with and without PFG's, the b-value in equation 3.1.5 must be calculated.

The b-value
[6]

The extra dephasing/rephasing caused by the PFG's depends on the gradient strength (G), the duration of the lobes (δ) and on the time between the beginning of the first gradient lobe and the second (Δ). The b-value is used as a value that describes the sensitivity of a measurement for diffusion caused by the PFG's, the higher the b-value, the more sensitive.
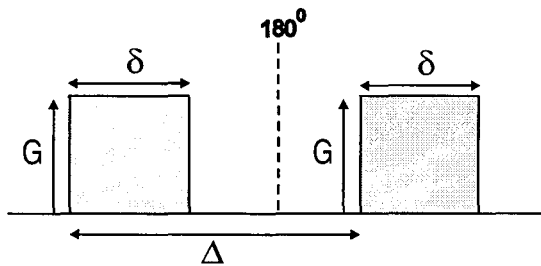
Figure 3.3: PFG's with square lobes.

When the PFG's have square lobes, as shown in Figure 3.3, then the b-value is given by:

$$b_i = \int_0^{TE} k_i^2(t)dt = \gamma^2 G_i^2 \delta^2 (\Delta - \frac{\delta}{3}) \qquad i = x, y, z$$

(3.1.6)

with
γ = the gyromagnetic ratio
δ = the duration of the gradient (rise time neglected)
Δ = time between the start of the first and the start of the second gradient
and x,y,z = the direction in which the PFGs are applied

In practice it takes time for the gradient to rise from zero to its maximum value, resulting in trapezium gradient lobes, as shown in Figure 3.4.
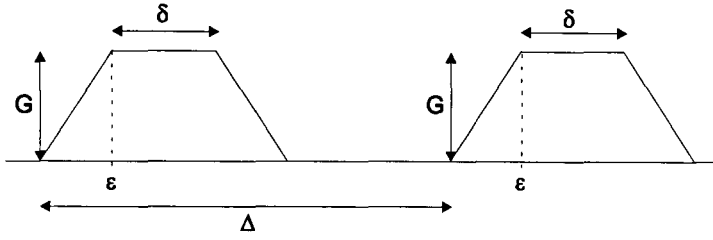
Figure 3.4: PFG's with trapezium lobes.

The b-value for this situation becomes:

$$b_i = \int_0^{TE} k_i^2(t)dt = \gamma^2 G_i^2 [\delta^2 (\Delta - \delta/3) + \varepsilon^3/30 - \delta\varepsilon^2/6] \qquad i = x, y, z \qquad (3.1.7)$$

with ε= rise time of the gradient

When the b-value is calculated, the ADC can be determined using equations (3.1.4 and 3.1.5), this is described in the next paragraph.

§3.2 The Apparent Diffusion Coefficient [6]

The ADC is a value that describes the average diffusion of water molecules in a volume unit (voxel) and differs for different tissues, see chapter 1.
It is called the Apparent Diffusion Coefficient because the water molecules are restricted by the tissue and cannot move freely.

Equation (3.1.5) contains two exponents. The first exponent, describing the decrease caused by T_2-*decay*, is equal to the exponent that is measured without PFG's (equation 3.1.4).
By dividing the signal measured with PFG's by the signal measured without PFG's the effect of T_2-decay is eliminated, rewriting gives:

$$ADC = -\frac{1}{b} \ln\left[\frac{S_b}{S_0}\right] \qquad (3.2.1)$$

The signal intensities S_0 and S_b can be measured in the image and the b-value can be calculated (3.1.6./3.1.7.), so with (3.2.1) the ADC can be determined.
At least two signals (two images) are necessary to determine the ADC, one measured with (S_b), and one measured without PFG's (S_0).
When instead of one, more signals with PFG's (each time for a different b-value) are measured, the ADC can be found by plotting $ln(S_b/S_0)$ against the *b-value*, the ADC is the slope of the line fitted through the data points (signal decay curve), as shown in Figure 3.5.
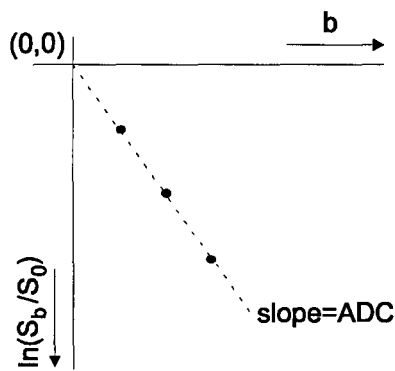
Figure 3.5: Determining the ADC when more than one b-value is used, the ADC is defined by the slope of the line fitted through the data points.

In clinical applications the PFG's are applied in three orthogonal directions x, y, z resulting in respectively an *M (=Measurement), S (Slice selection)* and *P (Phase encoding)* image. From these three images (*M, S, P*) an average image (isotropic) is calculated by

$$S_I = \frac{S_M + S_S + S_P}{3}$$ (3.2.2)

An *ADC* can be assigned to each voxel and each *ADC* coincides with a certain gray level (defined by a gray scale) for visualization. An example of an *ADC* image is given in Figure 3.6, the lighter the gray the higher the *ADC*.
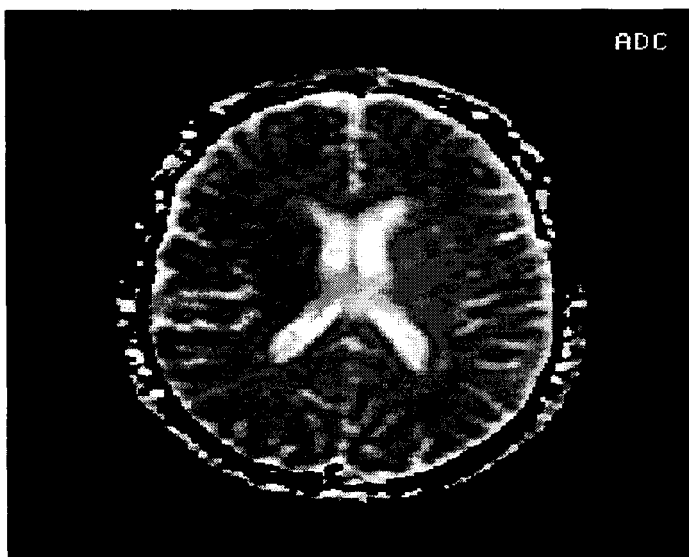
Figure 3.6: An example of an ADC image, the lighter the pixel, the higher the ADC.

§3.3 Diffusion Tensor Imaging
[6]

The principle of Diffusion Tensor Imaging is the same as in Diffusion Weighted Imaging, only the measurements are performed in six (*P, M, S, MP, PS* and *MS*) instead of three directions, making it possible to visualize the tissue structure.
By placing PFG's in two directions at the same time, the diffusion can be measured in the MP-, PS- and the MS-directions.

For tensor imaging equation (3.2.1) becomes

$$\ln\left(\frac{S_b}{S_0}\right) = -\sum_{i=1}^{3}\sum_{j=1}^{3} b_{ij} ADC_{ij} \tag{3.3.1}$$

with $i=1,2,3$ = the x,y,z direction respectively
         $j=1,2,3$ = the x,y,z direction respectively
         ADC_{ij} = the ADC value in the i,j direction
and b_{ij} = the b-value for the i,j direction

The ADC_{ij} matrix can be written out as:

$$ADC_{ij} = \begin{bmatrix} ADC_{xx} & ADC_{xy} & ADC_{xz} \\ ADC_{yx} & ADC_{yy} & ADC_{yz} \\ ADC_{zx} & ADC_{zy} & ADC_{zz} \end{bmatrix} \tag{3.3.2}$$

From equation (3.3.1) follows that the *ADC* measured with Diffusion Weighted Imaging equals the average of the trace of the ADC_{ij} matrix ($ADC_{xx}=M$, $ADC_{yy}=P$ and $ADC_{zz}=S$). The elements ADC_{ij} equal ADC_{ji}.

The b-value for each direction can be calculated with equation (3.1.6 or 3.1.7).

By DTI the eigenvalues and eigenvectors belonging to the ADC_{ij}-matrix are determined. These eigenvalues and eigenvectors are used to visualize the tissue structure, arrows or ellipsoids are commonly used for this, as illustrated in Figure3.7.
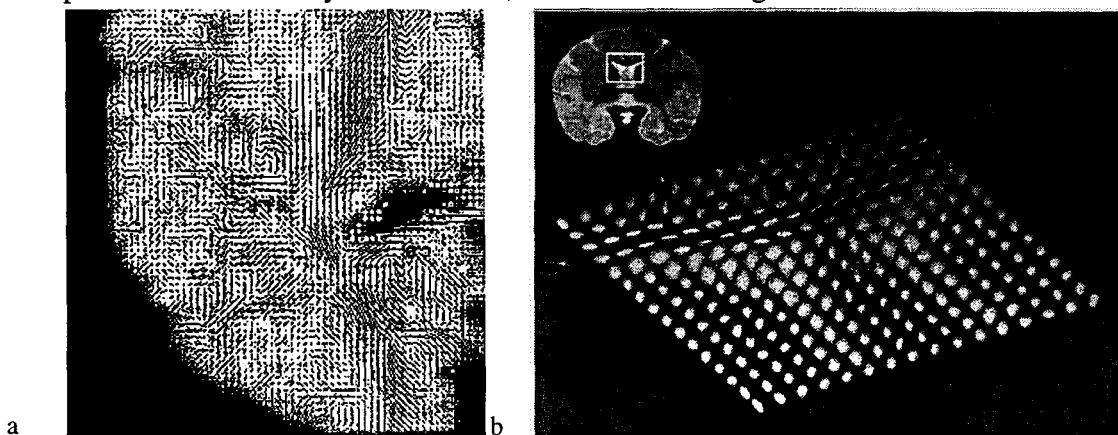
Figure 3.7: a) Tissue structure visualized using arrows [11]. b) The tissue structure visualized using ellipsoids [6].

22

Chapter 4
Normal values of brain tissue.

To use the ADC quantitatively for the classification of the phase of an infarct and to classify the brain development, there are two important conditions that need to be satisfied.
First, the ADC measured must be accurate, in order to use it quantitatively. How accurate the ADC should be depends on the application [8].
Second, the ADC's of healthy and ischemic tissue need to differ enough to be able to distinguish between them. By determining the ADC's of healthy and ischemic tissue and by determining the inter human variation, this can be examined.
In the first paragraph, the scans that are performed and the post-processing are discussed. The results (normal values) of the scans are presented in the second paragraph. In the third paragraph it is checked if the ADC depends on the number of b-values used and on which b-values are used. In the last paragraph the measurements are discussed.

§4.1 Groups

In this study the normal values of the ADC's for three different groups are determined: healthy volunteers, healthy newborns and newborns suffering from hypoxic ischemia. Why these groups are selected and which scans are made for each group is discussed for each group separately.
The ADC's are determined for White Matter (WM), Gray Matter (GM) and the Cerebro Spinal Fluid (CSF).

Healthy volunteers

A group of eleven healthy volunteers is used to determine the inter human variation and to investigate which and how many b-values should be used to determine the ADC accurately. Scans are made using 4 b-values (b=0,400,800,1200 s/mm^2).

For the determination of the inter human variation, the scans are processed using only three b-values (b=0,400,800 s/mm^2).
In the future the ADC's measured by the healthy volunteers are going to be used as a reference for values obtained in patients suffering from stroke.

Healthy newborns

Normal values of ADC's in tissue of healthy newborns are necessary to see whether there is a significant difference between the ADC's for healthy or ischemic tissue.
The ADC's found by healthy volunteers cannot be compared to the ADC's found by the newborns, because the tissue structures changes when the brain develops which can cause a difference of 20% in the ADC [8], therefore the ADC is determined by healthy newborns.
The scans are made using three b-values (b=0,400,800 s/mm^2), the protocol used is slightly different from the protocol used by the healthy volunteers.

The ADC's measured by newborns suffering from hypoxic ischemia are compared to the normal values found for healthy newborns, to determine the difference in the ADC. By these newborns the ADC is determined in ischemic tissue and in the same tissue measured contralateral. A difference of 40-50% is expected [8].
The scans are made with three b-values (b=0,400,800 s/mm^2), the protocol used is the same as for the healthy newborns.

The protocols that are used are listed in appendix A.

The scan-time should be short for the newborns suffering from hypoxic ischemia, because they are often unstable and their sedation should be kept short. For the healthy newborns and for the healthy volunteers the scan-time should also be held short. Increasing the number of b-values prolongs the scan-time, therefore the scans need to be optimized using as few b-values as possible.
The scans made with four b-values are used to see whether the ADC depends on the number of b-values used and on which b-values are used. The results are discussed in paragraph 3.

The ADC's are determined by drawing a Region-Of-Interest (ROI) in the tissue under investigation, the average ADC and the standard deviation within this region are given. For the healthy volunteers the ADC's are determined for the White Matter (WM), Gray Matter (GM) and the Cerebro Spinal Fluid (CSF), as illustrated in Figure 4.1, for the newborns the Gray Matter is measured at the Basal Ganglia, as illustrated in Figure 4.1. The values measured anterior left and right are averaged to one value, the same for the values measured posterior.
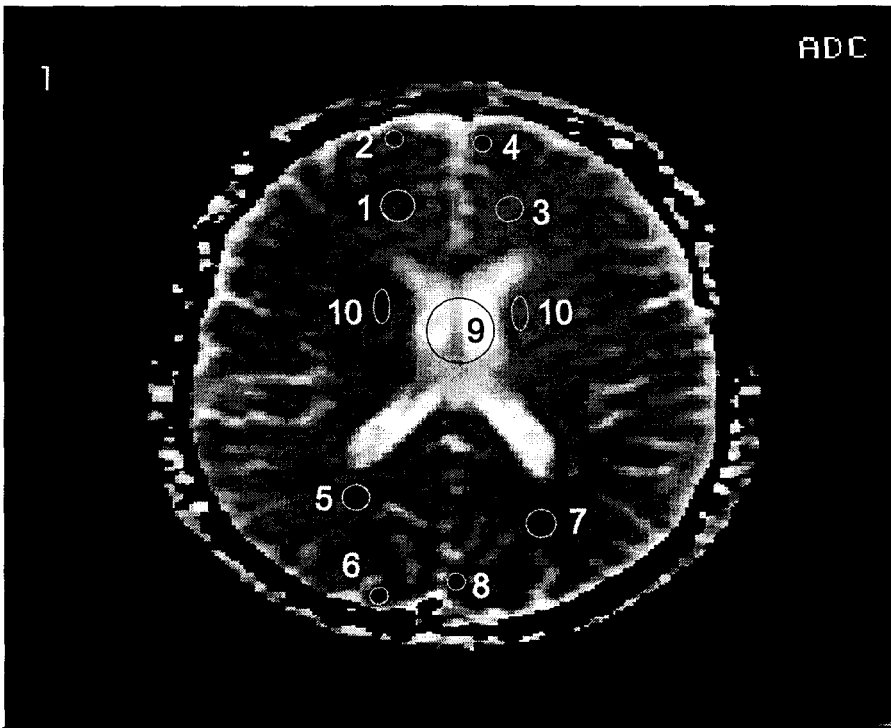
Figure 4.1: The locations where the ADC is measured.

1	WM left anterior	2	GM left anterior
3	WM right anterior	4	GM left anterior
5	WM left posterior	6	GM left posterior
7	WM right posterior	8	GM right posterior
9	CSF	10	Basal Ganglia

When the standard deviation is given as a percentage, is calculated as follows:

$$SD(\%) = \frac{SD(withinROI)}{average\ ADC} \tag{4.1.1}$$

§4.2 Normal values

Healthy Volunteers

The group of healthy volunteers consisted of 11 persons, 4 women and 7 man. The average age of the women was 23 and the average weight was 65.25 kg. The average age of the man was 27 and the average weight was 77.43 kg.
The averaged ADC's found are listed in Table 4.1, the complete list of ADC's that are measured is given in Appendix B.
All the volunteers gave a written informed consent for the measurements.
The ADC's are determined with a Matlab computer program.

Tissue	GM anterior $(\times 10^{-9}\ m^2/s)$	GM posterior $(\times 10^{-9}\ m^2/s)$	WM anterior $(\times 10^{-9}\ m^2/s)$	WM posterior $(\times 10^{-9}\ m^2/s)$	CSF $(\times 10^{-9}\ m^2/s)$
ADC±SD	0,84±0,03	0,84±0,02	0,74±0,05	0,74±0,03	3,41±0,27
SD (%)	3,28 %	2,19%	6,67%	4,24%	7,79%

Table 4.1: Averaged ADC's found for the healthy volunteers.

Healthy newborns

The healthy newborns were scanned at an age of 4 weeks and were not sedated. ECG stickers are used for the triggering. The parents have given a written informed consent for the scans.
The ADC's for the healthy newborns are determined using the software on the MR-scanner. J. Buijs, neonatologist and C. van Pul worked out the measurements, the average ADC's are listed in Table 4.2, the complete list with ADC's is given in Appendix B.

	Basal Ganglia $(\times 10^{-9}\ m^2/s)$	WM anterior $(\times 10^{-9}\ m^2/s)$	WM posterior $(\times 10^{-9}\ m^2/s)$	CSF $(\times 10^{-9}\ m^2/s)$
ADC±SD	0,76±0,07	1,06±0,12	1,03±0,08	2,41±0,20
SD (%)	9,08	11,09	7,38	8,22

Table 4.2: Average ADC's found for the healthy newborns.

The newborns suffering from hypoxic ischemia are scanned between 2 and 11 days after the onset of clinical symptoms and are sedated with chloralhydrate.

The ADC is determined at the position of the infarct, and if possible in the same tissue on the contra-lateral side. The averaged ADC's are listed in Table 4.3. When the ADC's are determined contra-lateral the same ROI is used as for the ischemic tissue.

The ADC is also determined at the same positions in the brain as by the healthy newborns, these ADC's are listed in Table 4.4. The complete lists with ADC's for Table 4.3 and Table 4.4 are given in Appendix B.

The measurements performed with two b-values (b=0, 400 s/mm^2) and with three b-values (b=0, 400, 800 s/mm^2) are listed separately.

J. Buijs, neonatologist and C. van Pul worked out the measurements on the MR scanner.

Number of b-values	Tissue	WM (x10^{-9} m^2/s)	WM contra-lateral (x10^{-9} m^2/s)	GM (x10^{-9} m^2/s)	GM contra-lateral (x10^{-9} m^2/s)
3	ADC±SD	0,48±0,17	0,80±0,26	0,52±0,04	1,01±0,17
3	SD(%)	36,81	31,98	7,39	17,33
2	ADC±SD	0,39±0,14	0,73±0,08		
2	SD(%)	36,76	11,29		

Table 4.3: Average ADC's found for the newborns suffering from hypoxic ischemia, the ADC's are measured at the ischemic tissue and contra-lateral

Number of b-values	Tissue	Basal Ganglia (x10^{-9} m^2/s)		WM anterior (x10^{-9} m^2/s)		WM posterior (x10^{-9} m^2/s)		CSF (x10^{-9} m^2/s)
		right	left	right	left	right	left	
3	ADC±SD	0,70±0,06	0,71±0,07	0,94±0,12	0,91±0,11	0,92±0,17	0,84±0,22	2,26±0,33
3	SD(%)	8,57	9,86	12,76	12,09	18,48	26,19	14,60
2	ADC±SD	0,59±0,06	0,64±0,07	0,87±0,09	0,91	0,74±0,15	0,77	1,42±0,15
2	SD(%)	10,17	10,94	10,34	-	20,27	-	10,56

Table 4.4: Average ADC's found for the newborns suffering from hypoxic ischemia, the ADC's are measured at the same position as by the healthy newborns.

The differences in the ADC's between healthy and ischemic tissue are 40-50%, as expected. The difference is large enough to distinguish ischemic tissue from healthy tissue, this is also illustrated in Figure 4.2.
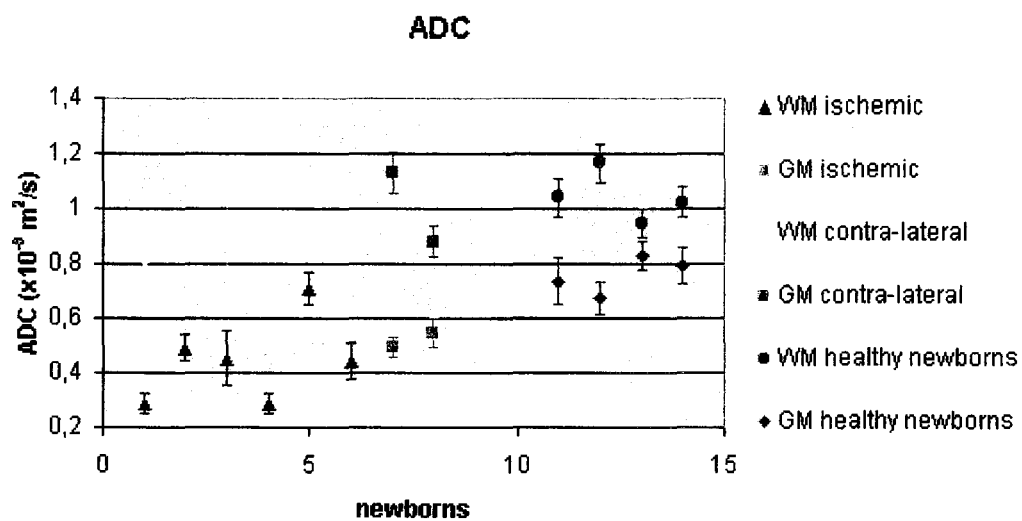
Figure 4.2: ADC's measured in ischemic tissue and in healthy tissue contra-lateral, and ADC measured by healthy newborns.

§4.3 ADC dependency on the b-value

To limit the scan time, the scans need to be made with as few b-values as possible. By the scans of the volunteers 4 b-values are used, to see if the ADC depends on the number of b-values and on which b-values are used. With a Matlab program the ADC's are determined in three different ways using:
-b=0,400,800,1200 s/mm^2
-b=0,400,800 s/mm^2
-b=0,400 s/mm^2
An example of the signal decay curve for White Matter by a volunteer is shown in Figure 4.3.
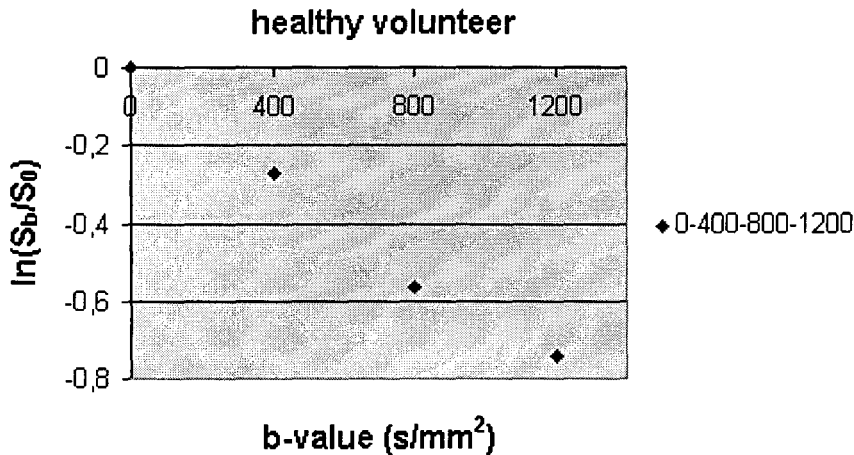
Figure 4.3: An example of a measurement with 4 b-values.

The points in the signal decay curve are not on a straight line; therefore the ADC will differ when a different number of b-values is used, as shown in Table 4.2.

b-values (s/mm^2)	ADC (x10^{-9} m^2/s)
0-400-800-1200	0,63
0-400-800	0,71
0-400	0,68

Table 4.2: ADC's found using a different number of b-values.

There is a difference of about 12% in the ADC's. For other tissue and scans made, there is also a difference in the ADC found depending on the number and which b-values used.

§4.4 Discussion

Inter-human variation

The standard deviation between the ADC found by the volunteers is for GM 2.7 %, for WM is 5.5% and for the CSF 7.8%.
By the healthy volunteers the inter human variation is small, possibly it can be used to compare differences in brain development by patients.

Ischemic versus healthy tissue

The measurements of the newborns suffering from hypoxic ischemia show that the ADC is significantly (40-50%) decreased in the ischemic tissues compared to the contra-lateral measurements. The ADC's measured contra-lateral, in the 'normal tissue', are slightly lower for WM compared to the healthy newborns. In the gray matter the ADC contra–lateral are slightly higher. What causes these slight differences is not known, maybe it is caused by the differences in the brain development
The 40-50% decrease in the ADC by hypoxic ischemia is larger enough to distinguish them.

Problems with the determination of the ADC

Drawing an ROI containing only one sort of tissue is very difficult. By Gray Matter it is likely that there is also CSF within the ROI, resulting in an overestimated ADC.
When the standard variation of the ADC within an ROI is large then it is likely that more than one tissue is present in the ROI.

The signal decay curve measured with 4b values by the healthy volunteers show that the points of the signal decay curve are not on a straight line, resulting in different ADC's when a different number of b-values is used for the determination.
Therefore, based on these measurements no conclusion can be given about the accuracy of the ADC, and no decision can be made about which and how many b-values should be used.

Conclusion

Before the ADC is used quantitatively and before a decision can be made which and how many b-values are going to be used, extra information is needed.
In the remaining part of this report, more information is gathered to examine whether the ADC is accurate enough to be used quantitatively, and to find out which and how many b-values should be used.

In the next chapter, factors that influence the ADC are discussed. For two of these factors correction methods are given in the following chapter.
Measurements are performed on a water phantom, an orange and on volunteers to see what happens to the ADC when different parameters belonging to the PFG's are changed. The scans and their results are presented and discussed in chapter 7.
The correction methods are used to see if they can improve the results of the measurements, their results are also presented and discussed in chapter 7.
In chapter 8 a conclusion on whether the ADC is accurate enough to be quantitatively is given, together with recommendations.

Chapter 5
Accuracy.

The ADC's measured by the healthy volunteers, as shown in chapter 4, depend on which and how many b-values are used. What causes this dependency needs to be examined, therefore a summation of the most important factors [8] that influence the ADC is given in this chapter. The factors can be divided in system factors and bulk sample factors. System factors are factors that are related to the hardware and software of the MR scanner itself, bulk sample factors are factors that are caused by the object that is imaged. The system factors are discussed first and second the bulk sample factors are discussed.

§5.1 System factors

The systems factors that cause inaccuracies can be divided in background imaging gradients, diffusion gradient amplitude and linearity, RF-pulses and noise. These inaccuracies will be explained here.

Background imaging gradients

The background imaging gradients are the slice selecting, the phase encoding and the read-out gradients. They can have two effects:
(1) they lead to diffusion signal losses in themselves (self-talk)
(2) they can interact with diffusion sensitizing gradients during the TE interval resulting in an increase or decrease of the diffusional phase coherence (cross-talk)
Background imaging gradients are the most significant source of inaccuracies in DWI, they can lead to errors up to 20%, [8].
The errors that arise are different for an isotropic and anisotropic medium and also for different directions of the diffusion sensitizing gradients (oblique, parallel or perpendicular). Especially in EPI-sequences, the background imaging gradients are known to cause large errors, therefore a correction method [9] is given in the next chapter. This correction method is used in chapter 7 to see whether the correction for the background imaging gradients improves the results.

Diffusion gradient amplitude and linearity

The area under Pulsed Field Gradient (A) should be equal to the area under PFG (B) when the gradients are calibrated correctly, as is shown in Figure 5.1. When the areas are not equal, the dephasing caused by the first lobe is not completely rephased by the second lobe, resulting in inaccuracies of the ADC. Gradient calibration involves the gradient amplitude (strength) and linearity, and can contribute to an inaccuracy up to 10%.
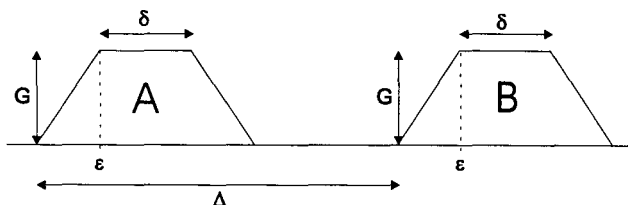
Figure 5.1: The area under the two PFG's should be equal.

For clinical systems gradient strengths are within 2% of their specified value at the isocenter of the magnet. This can lead to an error of 4% in the b-value, because it depends on G^2. The errors in the gradient strength can be caused by eddy currents or by spatial inhomogeneities.

Eddy currents can cause gradient imbalance leading to large errors in the gradient strength by diffusion imaging. They can also cause spatial misregistration in the Diffusion Weighted Image relative to the reference image. On most clinical systems actions are taken to reduce the eddy currents.

Spatial inhomogeneities cause spatial variation in the ADC. According to performance specifications, the spatial linearity of the gradients has a root-mean-square (rms) deviation of <1% over 45 cm which leads to spatial variations in ADC of <2% on top of the possible error at the isocenter. The closer the object is to the coil the larger the larger the error becomes.

RF pulses

Imperfections in the RF pulses, the 90^0 and 180^0 pulses, can be sources of error in the PFG method. Deviation in the 180^0 pulse can lead to accumulation of phase errors equivalent to diffusion gradient imbalance.

Noise

There are two sorts of noise: white noise in low signal areas and structured noise arising from system factors.

Noise can lead to an over estimation of the signal intensity, especially for low SNR.

The errors in the signal intensities caused by noise are different for different tissues and for different b-values.

In [10] a correction method is proposed to correct for the inaccuracy caused by noise. This correction method is discussed in more detail in the next chapter and is used to see whether the result can be improved.

In summary: the background imaging gradients form the largest source of errors (up to 20%), second the diffusion gradients (up to 10%). The other errors can add up to an error of 5%.

§5.2 Bulk sample factors

Besides the system factors described above there are also bulk sample factors that influence the accuracy. The bulk sample factors that cause inaccuracies are sample background gradients, subject motion and CSF/brain pulsatility and microscopic, biophysical sample factors. These inaccuracies will be discussed in this part accordingly.

Sample background gradients

Within the sample, susceptibility differences occur and there is a susceptibility difference between the sample and the surrounding air. These differences cause so called sample background gradients, which are 'on' during the whole echo-time.
The sample background gradients have a random direction and can be measured in order to determine their significance and to determine a region of interest for quantitative diffusion measurements.
The sample background gradients can be partly removed by active shimming.

Subject motion and CSF /brain pulsatility

There are patient movements and movements of the CSF. The movements of the CSF are a result of the pulsation of arteries caused by the beating of the heart. The patient's movement is non-periodic and the movements of the CSF are periodic. The artifacts can be reduced by signal averaging, by cardiac gating (each line in the k-space is measured at the same moment, determined by the heart rhythm of the patient) or by decreasing the scan time. These solutions reduce but not eliminate the artifacts.

Microscopic, biophysical sample factors.

Inaccuracies can also be caused by the presence of different biophysical properties inside one voxel. A cell does not contain only water, it also contains organelles, a cell-nucleus etc, resulting in different biophysical properties for each tissue. The diffusion is determined by these properties. When more biophysical properties are inside one voxel, a combined diffusion is measured.

Chapter 6
Correction methods.

From the measurements performed on the healthy volunteers followed that the ADC depends on the b-value that is used. Two system factors mentioned in chapter 5, have an important influence on the ADC for the EPI-sequence, the self- and cross-talk of the background imaging gradients and noise in the image; [8], [9] and [10]. Their correction methods are discussed in this chapter. In the first paragraph the correction for the self- and cross-talk between gradients is discussed. In the second paragraph the parameters that are related to the Signal-to-Noise-Ratio and the correction for the noise are discussed.

§6.1 Correction for the self- and cross-talk between gradients

Before explaining the correction method, the situation when the gradients do not interact is first discussed.
In this situation, the measured signal is attenuated, because the second PFG-lobe cannot rephase all the spins due to the diffusion (see chapter 3). The sensitivity of the measurements for diffusion is described by the b-value, equation (3.1.6). When the gradient strengths, duration and the time between the gradients are not influenced by the other gradients, the b-value from equation (3.1.6) describes the sensitivity correctly.

Suppose that the different background gradients do interact, they influence themselves and each other (self- and cross-talk). The b-value that is calculated with equation (3.1.6) does not represent the correct sensitivity anymore.
When the b-value is not corrected for this, it can lead to errors of 20% in the ADC [8]. A correction method is proposed ([9]) in which, for each measurement direction, a b-value is calculated taking the contributions of self- and cross-talk into account. The b-values for each direction are placed in a matrix, called b-matrix. When measurements are performed in six directions, the ADC can be determined using equation (3.3.1).

To determine the b-value in each direction, taking the self- and cross-talk into consideration, it is necessary to know all the gradient strengths, gradients duration and the times between the gradients. For the DW-EPI-sequence as used in the Saint Joseph Hospital, the time diagram is given in Figure 6.1.
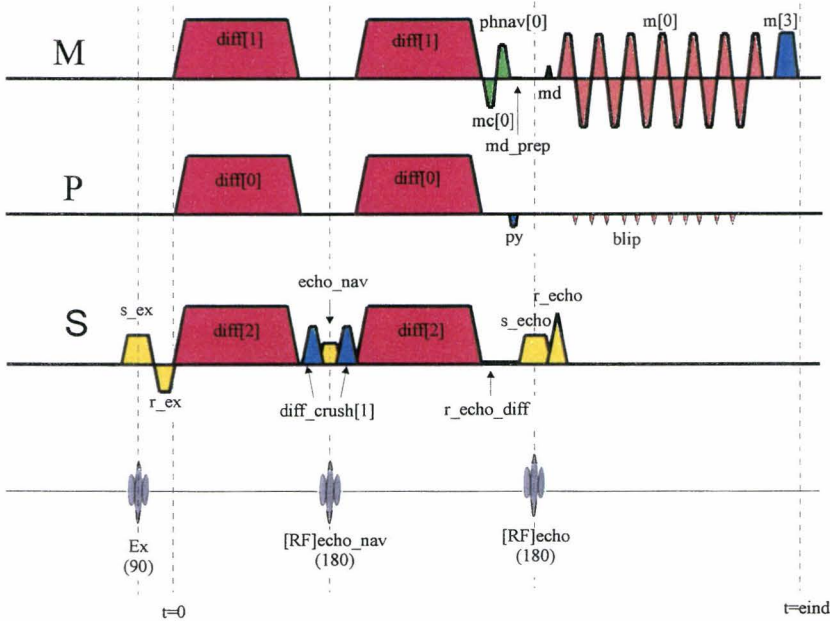
Figure 6.1: The DW-EPI-sequence used on the MRI scanner of the Saint Joseph Hospital.

The following gradients can be distinguished:
In the read-out direction (M):
        *the diffusion gradients, (diff[1])
        *a read-out navigator gradient , (mc[0] and phnav)
        *md_prep[1]
        *a small gradient (md)
        *the read-out train, (m[0])
        *a gradient after the read-out train, to make sure that the dephasing is complete before the next excitation (m[3])

In the phase direction (P):
        *the diffusion gradients, (diff[0])
        *py[1]
        *the phase encoding EPI-train, (blip)

[1]: due to md_prep and py the starting point in k-space is bottom right, a 180^0 pulse follows, causing the starting point to be at the upper left corner of the k-space.

In the slice selection direction (S):
        *the 90^0 slice selection gradient, (s_ex)
        *the refocusing, (r_ex)
        *the diffusion gradients (diff[2])[2]
        *the crusher gradients (diff_crush)[2]
        *the 180^0 slice selection gradient (echo_nav)
        *an extra 180^0 slice selection gradient is given, (s_echo)
        *an extra refocusing gradient, (r_echo)
[2]the two trapeziums lobes are treated as a pair in the calculation of the b-matrix.

For each gradient the self-talk must be calculated, and for the cross talk all the possible pair-wise interactions between gradients must be calculated, using equation 6.1.1.

$$b_{\alpha,\gamma} = \int_0^{TE} [k(t) - 2H(t-\tau) \cdot k(\tau)][k(t) - 2H(t-\tau) \cdot k(\tau)]dt \qquad (6.1.1)$$

with $2\tau = TE$,

$$k(t) = \int_0^t G_\alpha(t')dt' \qquad (6.1.2)$$

The functions $k(t)$ and $b_{\alpha,\gamma}$ are defined by Stejskal and Tanner with H the Heaviside function [8]. The parameters α and γ represent a gradient, for example the crusher gradient or the slice selection gradient. For the cross-talk, α represents one gradient and γ represents the other gradient, for self-talk $\alpha = \alpha$.

For each direction a b-value must be calculated. By placing all the gradients horizontal and vertical in a table (a part of such a Table is illustrated in Table 6.1) it is easy to see which contributions there are.

Table 6.1: A part of a table that can be used for the calculation of the b-values for each direction. The red line and blue line illustrate how gradients are canceled when they are not present in the i- or j-direction.

There are six directions (ij-directions); (PP=P, SS=S, MM=M, PS, MS and MP).
The b-values for the ij-direction can then be determined as follows.
Start for the i-direction and select the direction (P, M, S). Each gradient that is not present in this direction (for the sequence used) is canceled. This is done by pulling a vertical line through the column in which the gradient is placed, as illustrated by the red line in Table 6.1. Do the same for the j-direction, but pull now a horizontal line as illustrated by the blue line in Table 6.1.
Calculate the elements that are left over, their sum is the b-value for the ij-direction.

For each direction a b-value is calculated, in which the self and cross talk are taken into account, by dividing $ln(S_b/S_0)$ in each direction by the b-value belonging to that direction, there can be corrected for the self- and cross-talk.

Simplifying the b-matrix

The calculation of the b-values can be simplified, because some contributions are zero. According to [9] each gradient that is refocused has no effect on gradients that are coming later in time. Notice that in the EPI-sequence used, see Figure 6.1, the 180^0 slice selection gradient is given between the diffusion and crusher gradients, causing the second lobe to refocus the first lobe.
This means that the crusher gradients, the diffusion gradients and the navigator echo have no effect on the gradients that are coming after them. They do have an effect on the gradients applied during and in between their gradient lobes, and on themselves.

Md_prep, r_echo_diff and py are on for only a short time or with a low gradient magnitude, and can therefore be neglected in the calculation of the cross-talk of the b-matrix. In the calculation of self-talk they are not neglected.

The b-matrices for the different protocols and b-values

For the protocol used for healthy volunteers (TE_{diff}=100ms), the b-matrix is calculated for three different gradient strengths. For the protocol used for the healthy newborns and the preterm newborns with hypoxic ischemia (TE_{diff}=80 ms) the b-matrix is calculated for two different gradients strengths. Before correction, the b-values are the same in all the directions and are listed in Table 6.2. The b-values in each direction, after correction for the self- and cross-talk, are also listed in Table 6.2. How much the b-value is increased after the correction compared to for correction is placed in percentages under the b-value.

	protocol	healthy volunteers			newborns.	
	direction	b-value (s/mm^2)			b-value (s/mm^2)	
Before correction	all	1200	800	400	800	400
After correction	P	1201,59 (0.13%)	801,16 (0.14%)	400,74 (0.19%)	801,66 (0.21)	401,24 (0.31)
	M	1201,31 (0.11%)	800,84 (0.11%)	400,46 (0.12%)	800,84 (0.12)	400,56 (0.14)
	S	1254,54 (4.55%)	844,60 (5.57%)	431,78 (7.94%)	857,42 (7.18)	441,17 (10.29)
	MP	1201,27 (0.11%)	800,84 (0.10%)	400,42 (0.11%)	800,83 (0.10)	400,41 (0.10)
	MS	1219,45 (1.62%)	815,68 (1.96%)	410,92 (2.73%)	820,09 (2.51)	414,03 (3.51)
	PS	1219,48 (1.62%)	815,72 (1.96%)	410,96 (2.74%)	820,40 (2.55)	414,34 (3.59)

Table 6.2: The b-values before and after correction, for the protocol for healthy volunteers and for protocol for the healthy newborns and the newborns suffering from hypoxic ischemia.

In the MS, PS and the S-direction the increase in the b-value is more than 1%. The S-direction is corrected the most. The corrections (%) are higher for the protocol used by the newborns than for the protocol used by the volunteers.

§6.2 Noise

In chapter 5 noise is also mentioned as a system factor that influences the accuracy of the ADC. In [10] a correction method is discussed that corrects for the bias on the signal caused by noise. In this paragraph the scan parameters that influence the Signal-to-Noise-Ratio (SNR) are discussed first followed by the correction method.

Parameters that influence SNR

In this paragraph the parameters of the MR-scanner that can be varied by the operator, in order to optimize the SNR, are discussed.
Besides SNR, the resolution (R) and the scan time will also have to be optimized. The SNR, R and scan time have parameters in common (see equations 6.2.1, 6.2.2 and 6.2.3), [2][3], therefore optimizing one influences the others.
For patients comfort the scan time should be kept as short as possible, as long as the image quality is still acceptable for diagnosis.

The SNR is given by

$$SNR = (FOV_x)(FOV_y)\Delta z \sqrt{\frac{NSA}{N_x N_y BW}}$$
(6.2.1)

with: SNR = Signal to Noise Ratio
Ny = number of phase encoding steps
Nx = number of read-out steps
Δz = slice thickness
NSA = Number of Signal Averaged
and $FOV_{x,y}$ = Field Of View in the x- or y-direction

The resolution (R) is the minimum distance that can be distinguished between two points on an image and is determined by:

$$R = FOV/N$$
(6.2.2)

with N number of points per line.

The scan time for the EPI-sequence is given by:

$$\text{scan time} = TR \cdot N_y \cdot NSA / EPI_{factor}$$
(6.2.3)

with: Ny = number of phase encoding steps
TR = Repetition Time
and EPI_{factor} = number of phase encoding steps after the 180^0 refocusing gradient

Correction method

The determination of diffusion coefficients is very sensitive to the presence of noise. Especially at low SNR the pixel intensities of imaged objects can be considerable increased. Depending on the diffusion weighting, different noise biases are added to the signal, which results in different ADC-values.

In [10], a noise correction method is proposed. A difference between Gaussian and non-Gaussian distributed noise must be made. When it is assumed that the noise is Gaussian distributed a correction of the signal intensity of an image is possible. When it is assumed that the noise is non-Gaussian distributed the complex data belonging to an image is necessary for correction.

The signal intensities of the clinical system that are corrected in [10] almost correct to the calculated reference value. This indicates that for the clinical MR system the noise is Gaussian distributed [10].

In the image the mean intensity of the background signal (noise) B_{avg} and the mean signal intensity to be corrected S_{avg} are measured, as shown in Figure 6.2. For a representative mean intensity the ROI must be drawn over a sufficiently large region on the image.
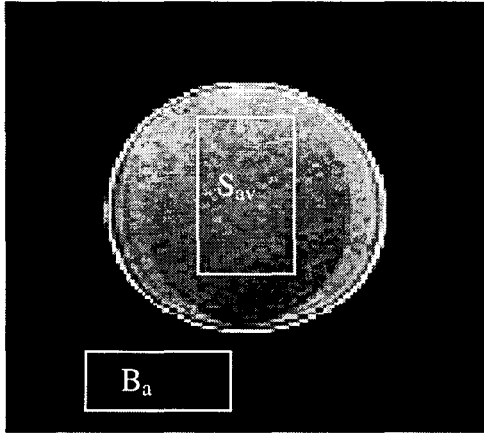
Figure 6.2: An example of a water phantom. Within the ROI drawn, the average ADC's are calculated to determine B_{avg} and S_{avg}.

By using an iterative algorithm, the signal intensity not influenced by noise (S) can be calculated.

For Gaussian noise [10], with a variance σ^2, the pixel intensity (S) becomes S_{avg}, a signal intensity biased by noise:

$$S_{avg}(S,\sigma) = \sigma\sqrt{\frac{\pi}{2}}\exp\left(-\frac{S^2}{4\sigma^2}\right)\left[\left(1+\frac{S^2}{4\sigma^2}\right)I_0\left(\frac{S^2}{4\sigma^2}\right)+\frac{S^2}{2\sigma^2}I_1\left(\frac{S^2}{4\sigma^2}\right)\right] \quad (6.2.4)$$

I_0 and I_1 in equation (6.2.4) are Bessel functions of the zeroth and the first order.
The variance σ^2 can be calculated from the background signal intensity, as shown in equation (6.2.5)

$$\sigma = \sqrt{\frac{\pi}{2}}B_{avg} \quad (6.2.5)$$

The background signal intensity B_{avg} and the average pixel intensity, S_{avg}, can be measured in the image, as shown in Figure 6.2. Using an iterative algorithm the signal intensity that is not influenced by noise (S) can be calculated using equation (6.2.4). The signal intensities of the images measured with PFG's and without PFG's are corrected separately, after which the ADC is calculated. When the B_{avg} is higher than S_{avg} no correction is possible.

The SNR ratio is defined by:

$$SNR = \frac{S_{avg}}{B_{avg}} \qquad\qquad (6.2.6)$$

with: S_{avg} =   ADC-value of the tissue, the water or the orange
and B_{avg} =   ADC-value of the background of the image

The results of the two correction methods will be discussed in chapter 7.

Chapter 7
Diffusion Weighted Imaging measurements.

To check whether the ADC is accurate enough to be used quantitatively, measurements are performed on the 1.0 Tesla MR-scanner (release 6.7; with diffusion key open) at the Sint Joseph Hospital in Veldhoven, the Netherlands. In the first paragraph it is discussed how the parameters, belonging to the PFG's, can be varied. This paragraph is followed by a description of the scans that are made. The results of the scans are given in paragraph 3, followed by a paragraph in which the results are discussed. The two correction methods are used and discussed in paragraph 5 and 6 respectively.

§7.1 PFG's parameters

The parameters of the PFG's that can be varied are shown in Figure 7.1, with:
-G, the gradient strength
-Δ, the time between the beginning of the first PFG and the beginning of the second PFG
-δ, the time that a PFG is on at maximum strength
-ε, rise time of the gradient
-*interval*, the time between the two PFG's
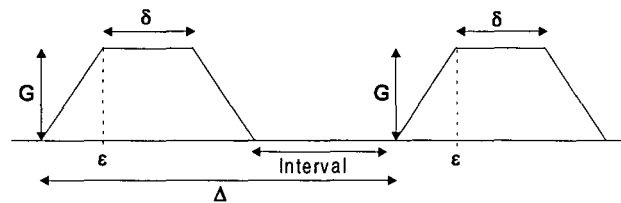
Figure 7.1: the parameters belonging to the Pulsed Field Gradients that can be varied.

A scan can be started in the normal operating mode and a scan can be started from the sequence development mode. When a scan is started in the normal operating mode, the b-value can be changed by varying the parameters TE_{diff} and the maximum b-value.
TE_{diff} defines the time available for the PFG's, therefore Δ and δ of the PFG's depend on TE_{diff} as follows:

$$\Delta = \frac{1}{2} \cdot TE_{diff} \tag{7.1.1}$$

$$\delta = \frac{1}{2} \cdot TE_{diff} - 2\varepsilon - \text{interval} \tag{7.1.2}$$

The b-value depends on Δ and δ, therefore a higher b-value can be reached when TE_{diff} is increased.
By using the sequence development mode, Δ and δ can be varied independently of TE_{diff}. The range in which the parameters can be varied is listed in Table 7.1

Parameter	Range
Δ	8,9988-140,2012 ms
δ	0-65,2012 ms
Interval	8,9988-140,2012 ms
ε	0,2 (TE_{diff}=125ms)-0,4(TE_{diff}=150ms) *

Table 7.1: Range of the parameters of the PFG's.
ε can be made 0,2 ms, but this limits the range of TE_{diff} and thus the range of Δ and δ. Therefore only ε=0.4 ms is used.

§7.2 Measurements

As described in chapter 1, the main question of this study is whether the ADC can be used quantitatively. After measuring the normal values, see chapter 4, this question remained. Therefore, different measurements are performed to check the influence of the scan parameters on the ADC. The correction methods, described in chapter 6, are used to see whether the results can be improved.

The scans that are performed can be divided in:
- G-variation, this can be done by changing the maximum b-value in the normal operating mode, Δ and δ are kept constant
- δ-variation, this is done by using the sequence development mode in order to keep Δ and G constant.
- Δ-variation, this is done by using the sequence development mode in order to keep δ and G constant.
- Scans in six directions, on the water phantom, to see whether the ADC depends on the protocol used.

The measurements are performed on a water phantom, an orange and a volunteer.

The water phantom is used because it is an isotropic medium, therefore the diffusion in all directions is the same. In the middle of the bottle the diffusion is not disturbed by boundaries. The water bottle that is used contains the following solution:

1000	ml demi-water
770	mg $CuSO_4.5H_2O$
2000	mg NaCl
1	ml arquad (1% solution)
0.05	ml H_2SO_4-0.1 N solution

This solution is used because the T1 (330 ms) and T2 (300 ms) for this solution can be compared to those of tissues, while the ADC is the same as for water.

The orange is used to get an impression about the influence of a structure on the ADC and to see if by changing the parameters a distinction can be made between restricted and unrestricted diffusion.
The cell sizes of an orange are estimated using a microscope, the cells sizes are illustrated in Figure 7.2.
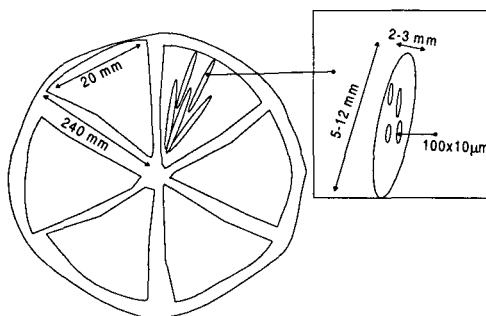

Figure 7.2: The cell sizes of an orange.

There are also scans performed on the brain of a healthy volunteer. These scans were made to see the influence of the parameters on the ADC when the diffusion is anisotropic. And to see whether the difference between restricted and unrestricted diffusion can be measured.

Processing of the data

All the measurements are worked out with a Matlab program, because the software on the MRI-scanner is protected.

The points in the signal decay curves are an average of $ln(S_b/S_0)$ measured in a ROI, each point has its own Standard Deviation (SD). The correlation coefficient (r^2) is used to display the degree in which the points coincide with the line drawn for the determination of the ADC.

For high b-values (b>1600 s/mm^2) the signal decay curve levels off. The points for b>1600 s/mm^2 are neglected in the determination of the ADC.
The point (0,0) (= $ln(S_0/S_0)$), is used as a point in the signal decay curve, but the line drawn for the determination of the ADC is not forced through this point. In this way the degree of freedom for the line is higher. Another reason not to use the point (0,0) is that for these measurements no PFG's are applied, making it a different sort of measurement.

The ADC of the water phantom depends on the temperature of the bottle, as shown in Figure 7.3 [7]. It is assumed that the water phantom has approximately the same temperature during all measurements, therefore the ADC is the same for all these measurements.
The temperature of the water phantom is 17-18 degrees, resulting in an ADC of between 1.69-1.74 $\times 10^{-9}$ m/s^2.
Taking small temperature variations in account, a standard deviation of 5% between the ADC's measured for the water phantom is considered to be acceptable.
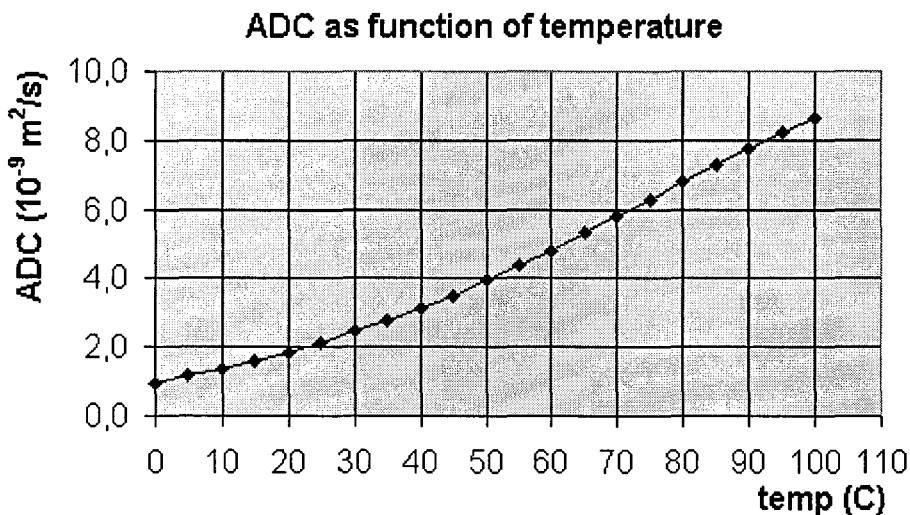

Figure 7.3: the ADC value as function of temperature, for a water phantom [7].

Differences between ADC's are calculated as follows:

$$difference = \frac{ADC_{max} - ADC_{min}}{ADC_{min}} x100$$ (7.2.1)

When the SD is given as a percentage then it is as follows:

$$SD(in\,\%) = \frac{SD}{ADC_{average}}$$ (7.2.2)

43

§7.3.Results

In this paragraph the results of the scans, described in the previous paragraph, are given. The results of the G-, Δ- and δ-variations are discussed followed by the results of the scans performed on the water phantom in six directions.

G-variation

By changing the gradient strength (G) the b-value can be varied. For the water phantom and the orange this is done for TE_{diff}=150,125,100 and 75 ms. For the volunteer the measurement is only done for TE_{diff}=150ms. The signal decay curves for TE_{diff}=150ms and TE_{diff}=75 ms are given in Figures 7.4 and 7.5.
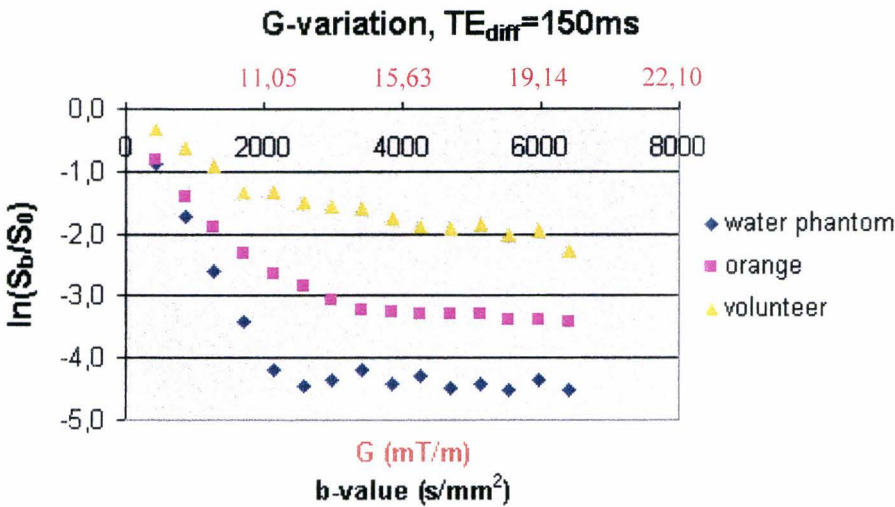

Figure 7.4: G-variation for a water phantom, an orange and a volunteer with δ=65.2012 ms and Δ=75 ms.
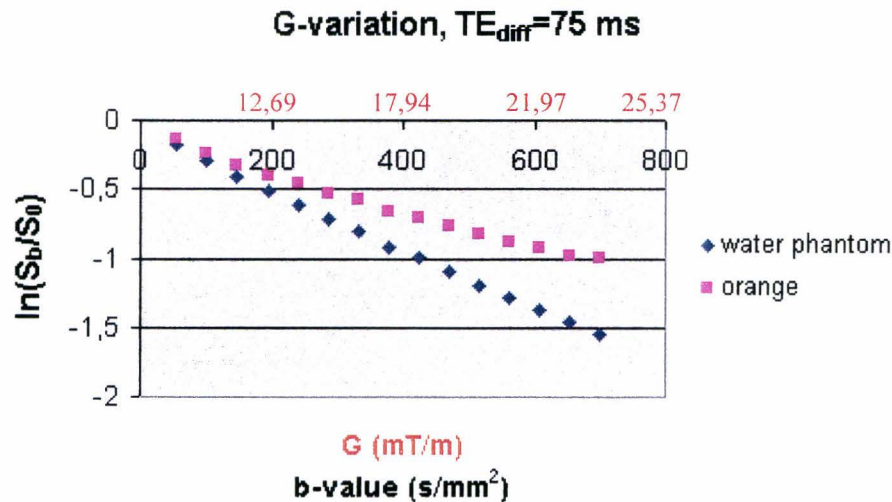

Figure 7.5: G-variation for a water phantom and an orange with δ=27.7012 ms, Δ=37.5 ms.

The ADC found for these measurements are plotted in Figure 7.6.
All the ADC's that are measured with the G-variation are listed in Appendix C.

ADC
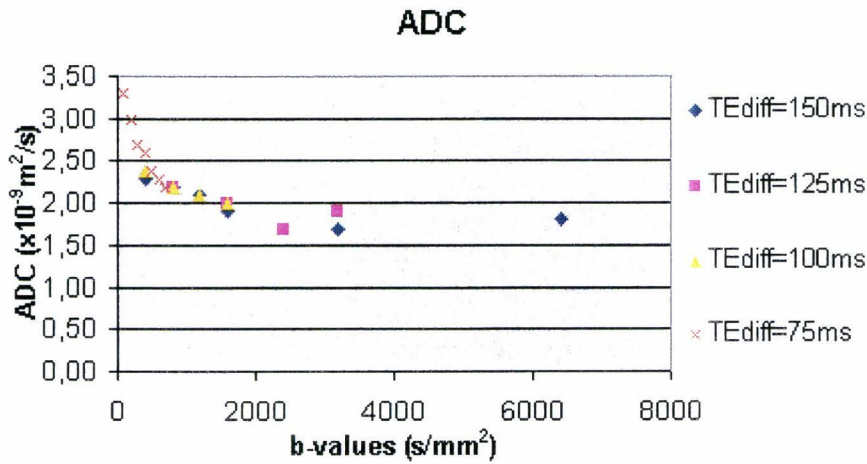
Figure 7.6: ADC's found for the water phantom found by the G-variation for different TE_{diff}. The ADC's are plotted as a function of the maximum b-value.

Remarks[1]:

- ◆ The scans by the volunteer are not performed for different TE_{diff}, due to new software that was installed on the MRI scanner. With this new software the parameter TE_{diff} cannot be varied anymore.
- ◆ The ADC measured for the orange for TE_{diff}=150 ms and TE_{diff}=125,100,75 ms cannot be compared because two different oranges were used.
- • The signal decay curves for the volunteer, the orange and the water phantom all three have the same tendency. They level off for b>1600 s/mm^2.
- • The bending points are less pronounced in the signal decay curve of the orange and the volunteer as for the water phantom.
- • The ADC's found for the water phantom for low maximum b-values is almost two times larger than the ADC found for high maximum b-values.
- • When the ADC's of the orange measured with TE_{diff}=150 are compared a difference of 66% is found, when the ADC's measured with TE_{diff}=125,100,75 ms are compared the difference is 300%.

[1]there are two sorts of remarks, those labeled with ◆ represent a remark about the way that the measurements are performed, those labeled with • represent a remark about the results.

Δ-variation

By varying Δ, the b-value can also be changed. Using the sequence development mode, Δ can be varied independent of TE_{diff}, the other parameters that determine the b-value are kept constant. The variations are done for different δ=5.2012, 10.2012 and 20.2012 ms. The signal decay curves are shown in Figure 7.7 to 7.9
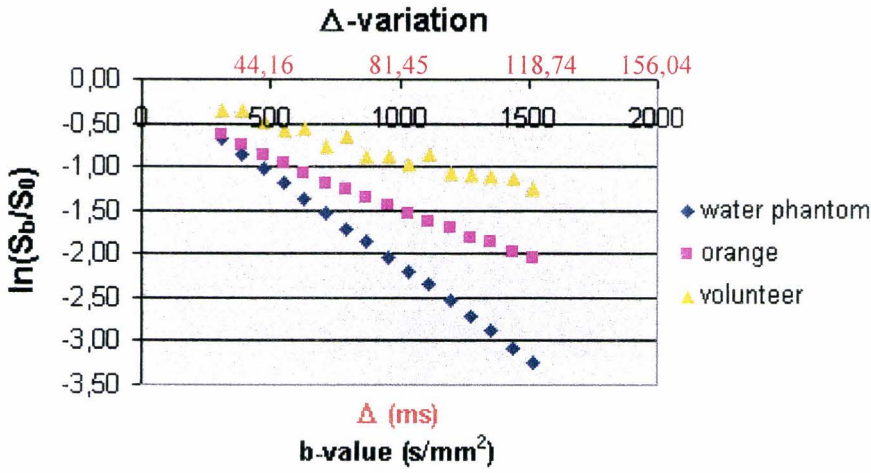
Figure 7.7: Δ-variations for δ=20.2012 ms and G=20.9988mT/m.
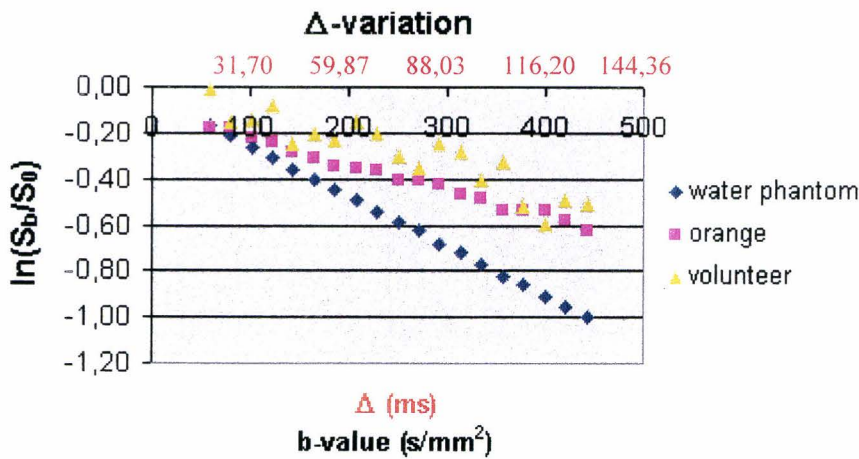
Figure 7.8: Δ-variations for δ=10.2012 ms and G=20.9988mT/m
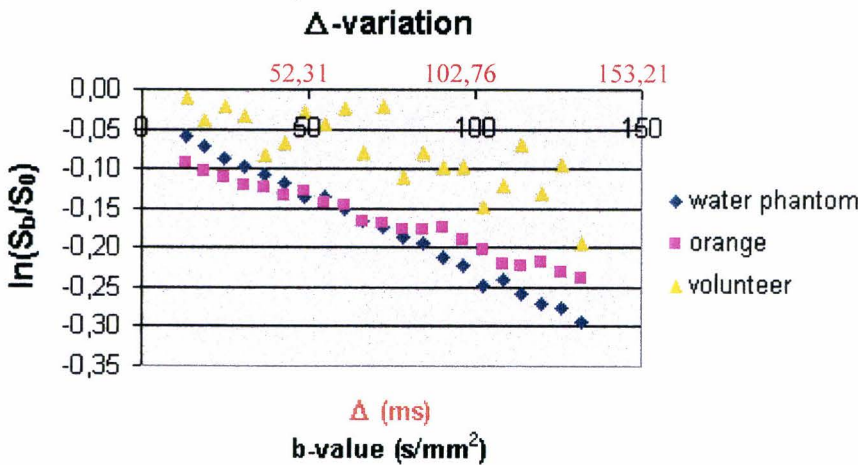
Figure 7.9: Δ-variations for δ=5.2012 ms and G=20.9988mT/m.

The ADC's that are found for these measurements are listed in Table 7.2.

	δ=5.2012 ms		δ=10.2012 ms		δ=20.2012 ms	
	ADC (x10^{-9} m^2/s)	r^2	ADC (x10^{-9} m^2/s)	r^2	ADC (x10^{-9} m^2/s)	r^2
Water phantom	1,96	0,998	2,18	0,999	2,11	0,999
Orange	1,21	0,984	1,13	0,988	1,16	0,997
Volunteer	1,02	0,614	1,31	0,858	0,74	0,953

Table 7.2: The ADC's found by the Δ−variations.

Remarks:

- The b-values that can be reached are below b=1600 s/mm^2, therefore no off leveling is seen in the signal decay curves
- When the ADC's that are found for the water phantom are compared a difference of 11.5% is found.
- When the ADC's that are found for the orange are compared a difference of 6.4% is found.
- When the ADC's that are found for volunteer are compared a difference of 77.5% is found. The signal decays for δ=5.2012 ms and δ=10.2012 ms are not coherent enough for the determination of ADC's, as can be seen from the low correlation coefficients (see Table7.2).
- The signal decay curves for the orange and the water phantom have the same tendency

δ-variation

By varying δ, the b-value can also be changed. Using the sequence development mode, δ can be varied independent of TE_{diff}, the other parameters that determine the b-value are kept constant. The signal decay curves are shown in Figure 7.10.
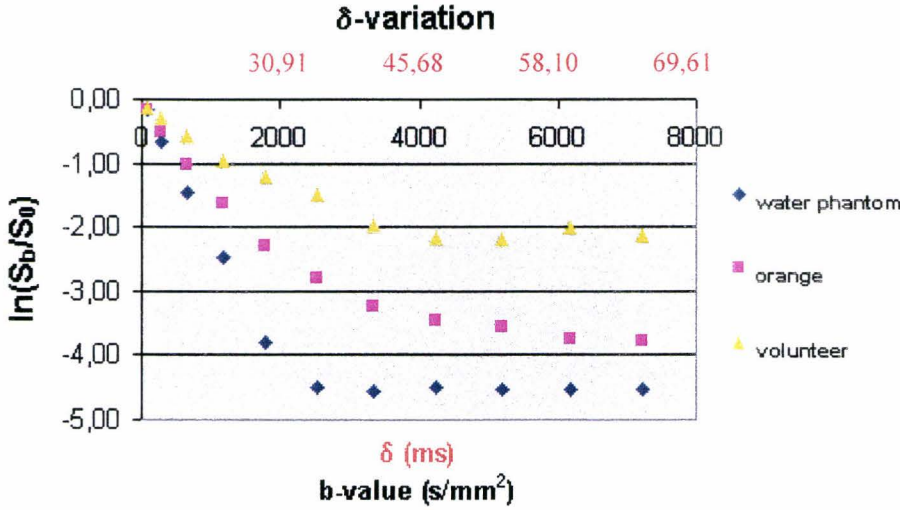
Figure 7.10: δ-variations done on a water phantom an orange and a volunteer with G=20.9988 mT/m and Δ=75 ms.

The ADC's are given in Table 7.3, the points that bend towards a horizontal line are neglected.

	ADC $(x10^{-9} m^2/s)$	r^2
Water phantom	1,83	0,984
Orange	1,08	0,986
Volunteer	0,56	0,975

Table 7.3: ADC's measured for a water phantom, an orange and a volunteer for the δ-variation.

Remarks

- The signal decay curves for the water phantom the orange and the volunteer, show the same tendency.

The differences in ADC's measured for the G-,Δ- and δ-variations for $b_{maximum}\approx1600$ s/mm^2 are illustrated in Figure 7.11. The difference between the ADC's for the orange are caused by the use of different oranges.

ADC for different variations
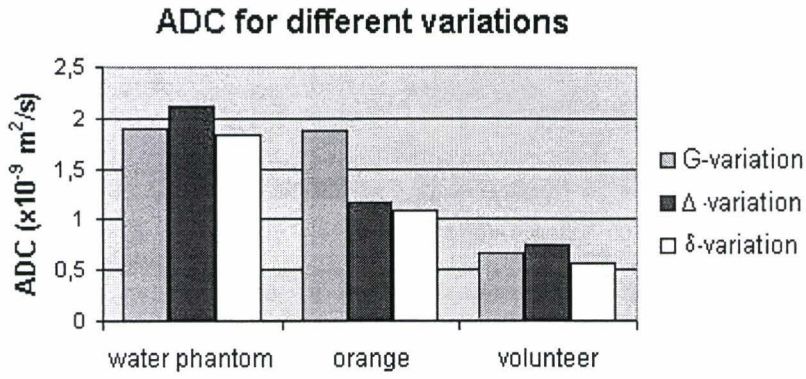
Figure 7.11: The differences in ADC measured with the G-,Δ- and δ-variation

Measurement in six directions

The water phantom is an isotropic medium, this means that the diffusion measured in all directions should be the same. By performing measurements in six directions it is checked if the diffusion measured is the same, or not. Especially for DTI it is important the ADC's, found for the water phantom, in all the directions are the same.

The measurements are performed using the protocols for the healthy volunteers and the protocol for the newborns (see appendix A), in this way it is also checked whether the ADC depends on the protocols. For the protocol used by healthy volunteers the scans are made with b=0,1200 s/mm^2, b=0,800 s/mm^2 and b=0,400 s/mm^2, for the protocol used for the newborns b=0,800 and b=0, 400 s/mm^2 are used.

All the ADC's are an average of the ADC's found within a region of interest.

For each measurement only the maximum and minimum ADC's that are found are given, together with the SD and the direction in which they are found, the results are listed in Table 7.4.

Protocol for the healthy volunteers				
B (s/mm^2)	Maximum ADC (x10^{-9} m^2/s)	Direction	minimum ADC (x10^{-9} m^2/s)	Direction
0-1200	2,25±0,33	MS	2,20±0,35	MP
0-800	2,39±0,30	PS	2,30±0,28	M
0-400	2,57±0,25	S	2,45±0,27	MP
Protocol for the newborns				
0-800	2,18±0,78	PS	2,10±0,70	P
0-400	2,51±1,15	P	2,26±0,94	MS

Table 7.4: Results of measurements performed in different directions for different protocols and b-values.

Remarks

- The standard deviations of the ADC's, within the ROI, found for the protocol for the newborns are large.

    Using b=0, 400 (s/mm^2) the standard deviation is 40-46% of the ADC value.

    Using b=0, 800 (s/mm^2) the standard deviation is 33-36% of the ADC value.

    The standard deviations for the protocols for the volunteers are 10-16% of the ADC value.

- When the maximum and minimum ADC are compared for each measurement separately, the difference is smaller than 5%, except for the measurements using b=0, 400 s/mm^2 there the difference is larger than10%

- When all the ADC's in Table 7.4 are compared a difference of 22.5% is found

- The average ADC in the P, S and M directions is determined for the measurements, when they are compared a difference of 18.44% is found.

§7.4 Discussion

Water phantom

The ADC's measured for the water phantom, using different parameters, should all be the same. The measurements on the water phantom are used to see whether the ADC is accurate enough to be used quantitatively.
Two things need to be taken into account:
-the differences between the ADC's for the G-, Δ- and δ-variations.
-the standard deviations of the points in the signal decay curves
Taking small temperature differences in account, a 5% standard deviation between the ADC's is considered to be acceptable.

The ADC's that are found by the G-variation for low maximum b-values are almost two times as large as those found for high maximum b-values. When the ADC's are compared for the Δ-variation a difference of 11.4% found. When the G-,Δ- and the δ-variations are compared the ADC's found differ 13.4% (the ADC's that are compared, are determined by approximately the same maximum b-value).
The ADC's are higher than those found in literature [7].

The standard deviations of the ADC within an ROI must also be considered.
By the G-variation there are only a couple of scans for which the standard deviations of the points within the ROI are below 5%. The range of the b-values, for which the SD is lower than 5%, depends on TE_{diff} and on the gradient strength. It is remarkable that the range of b-value that can be used, increases when a higher maximum b-value is given in, when the rest of the scan-parameters are not changed.
By the measurements with the Δ-variation the G-value is held constant 20.9988 mT/m the range of the b-value depends now on the δ used.
For all variations, the standard deviation (within an ROI) for b<100 s/mm^2 is higher than 10% and can reach up to 100%. Therefore b-values lower than 100 s/mm^2 should not be used.

From these results it can be concluded that the differences between the ADC measured are larger than the 5% acceptance level.

The measurements in six directions are performed using the protocol for the newborns and using the protocols for the volunteers.
From the measurements performed in six directions it follows that the ADC's measured in different directions differ less than 5%. When the ADC's measured in all directions, using different protocols are compared a difference of 22.5% is found.
The average ADC's (of the P, M and S-direction) are also determined for each measurement. When they are compared a difference of 18.44% is found. The high standard deviations within the ROI found for the protocol of the newborns for b=400 s/mm^2 are remarkable.

Orange and volunteer

The scans of the orange were made to get an impression of the influence of a structure on the ADC. The structure limits the diffusion resulting in a lower ADC, but the tendency of the signal decay curve remains the same as for the water phantom.

When the signal decay curve levels off for White Matter in the brain, the leveling is also seen for the water phantom and the orange, therefore the leveling is caused by noise and not by the difference in the diffusion of intra- and extra-cellular water as suggested in [12] and [13].

The scans of the volunteer were made to see what influence the parameters have on the ADC by anisotropic diffusion. Varying different parameters does not cause a different tendency in the signal decay curve. The correlation coefficients are lower for the lines drawn, maybe this is caused by movement of the volunteer or by the low SNR.

Difficulties by determining the ADC's

For high b-values (b>1600 s/mm^2) the signal decay curve levels off, points after the off leveling are neglected in the determination of the ADC. The exact bending point is difficult to determine, causing a extra inaccuracy of the ADC.

The drawing of an ROI on the image made of a volunteer is difficult: the ROI's are drawn on the image that is measured without diffusion, and even then it is likely that there are two sorts of tissues inside one ROI.

§7.5 Results of the correction using the b-matrix

The ADC measured in six directions differs for the water phantom, while the ADC should be the same in all directions. The differences for the ADC in the directions for b=400 s/mm^2 are over 10% and the differences between protocols is 22%, see Table 7.4.
In each direction different gradients are on, therefore the b-matrix might be useful to correct for the differences found in the directions. The difference between the protocols lies in gradient strengths, duration and time between the gradient, therefore the b-matrix might correct the differences between protocols.
The measurements performed on the water phantom in six directions, described earlier, are corrected using the b-matrix.
In Figure 7.12 an example of an uncorrected and a corrected measurement is given, the b-value for the measurement without correction was b=400 s/mm^2.

Diffusion in six directions

◆ without correction
■ with correction
ADC (without)=2.45±0.05 (x10^{-9} m^2/s)
ADC (with)=2.46±0.04 (x10^{-9} m^2/s)
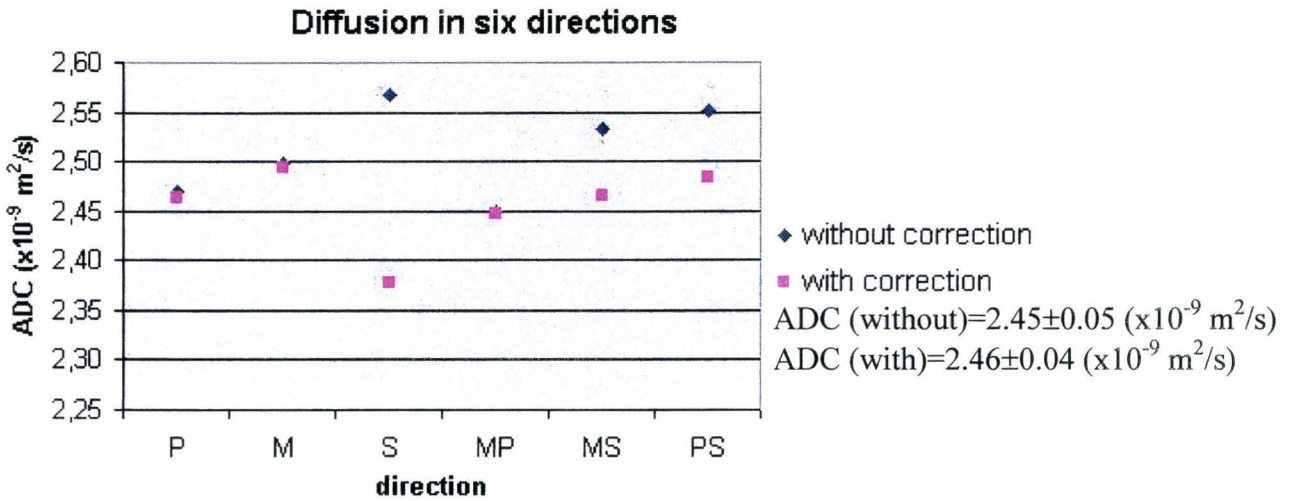
Figure 7.12: An example of a measurement with and without correction using the b-matrix.

The maximum and minimum ADC (together with the SD and the direction in which they are found) of each measurement after correction are listed in Table 7.5

B (s/mm^2)	Maximum ADC (x10^{-9} m^2/s)	Direction	minimum ADC (x10^{-9} m^2/s)	Direction
Protocol of the healthy volunteers				
1200	2.22±0.33	M	2.14±0.30	S
800	2.36±0.29	MP	2.24±0.29	S
400	2.49±0.28	M	2.38±0.23	S
Protocol used by the newborns				
800	2.12±0.41	PS	2.01±0.65	S
400	2.49±1.04	MS	2.19±0.91	MS

Table 7.5: ADC's for the different protocols after they are corrected for the self-talk and cross-talk.

Discussion

When all the ADC's measured using different protocols are compared a difference of 25% is found. When the averaged ADC's of the P, S and M directions are compared a difference of 18.44% is found. Compared to the differences found between the ADC's measured before correction (Table 7.4) there is no improvement.

The S-direction is corrected the most, resulting in a too low ADC compared to the ADC in the other directions. In Table 6.2 it can already be seen that the b-value in the S-direction is corrected the most.

The correction method does not improve the measurements, apparently the sequence is designed taking self- and cross-talk in consideration, therefore they do not cause the difference in ADC's.

§7.6 Results of the noise correction

The ADC values found by a G-, Δ- and δ-variation deviate from one another. In this paragraph we corrected for the bias caused by noise. These results are discussed first. For measurements in six directions the ADC differed depending on the b-value used, these measurement are also corrected they are discussed secondly.
At last an overall discussion is given about the correction.

G-, Δ- and δ-variations

In Figure 7.5 and 7.10 it can be seen that the signal decay curve levels off for high b-values. According to [10] these measurements can be improved by using the correction method, because the SNR is low for high b-values. The SNR of a measurement on a water phantom, with TE_{diff}=150ms and b=3200 s/mm^2, is given in Figure 7.13. In Figure 7.14 the signal decay curve before and after correction of this measurement is given.
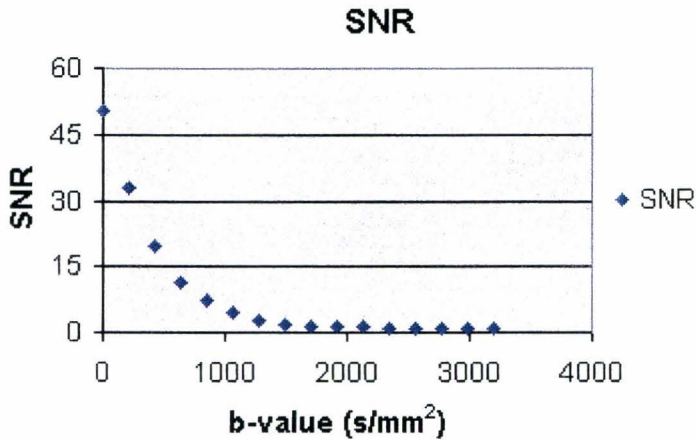
Figure 7.13: The SNR for a measurement on a water phantom with TE_{diff}=150ms and b=3200 s/mm^2.
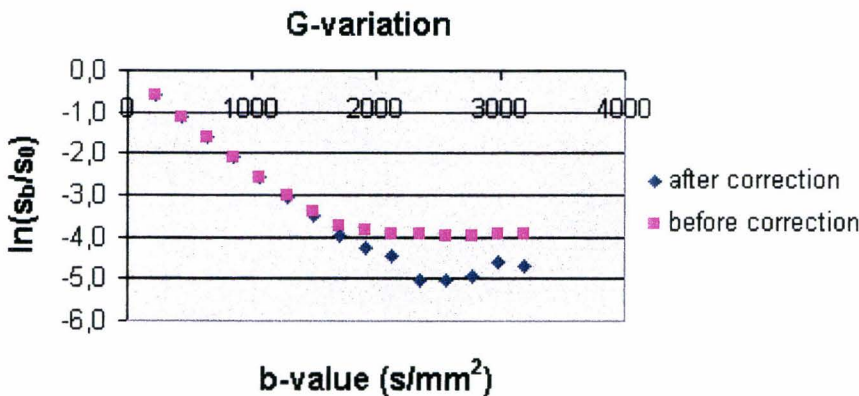

Figure 7.14: The signal decay curves before and after the influence of noise is corrected

As can be seen in the Figure 7.14 more points can be used to determine the ADC after the correction. The ADC is now determined for both the signal decay curves in Figure 7.14 using different numbers of b-values, the result are given in Table 7.6.

55

After correction		Before correction		
ADC $(\times 10^{-9}\ m^2/s)$	r^2	ADC $(\times 10^{-9}\ m^2/s)$	r^2	for b (s/mm^2) up to
1.97	0.985	1.51	0.913	2561
2.07	0.992	1.66	0.943	2348
2.10	0,990	1.83	0,967	2135
2.21	0,997	1.99	0,985	1922
2.27	0,999	2.13	0,996	1709
2.28	0,999	2.21	0,998	1496
2.30	0,999	2.26	0,999	1283

Table 7.6: ADC's for both signal decay curves in Figure 7.14, using different numbers of b-values.

As can be seen from Table 7.6, more points can be used for the determination of the ADC and the correlation coefficient is higher. The ADC's found after the correction are higher than before the correction.

When a signal decay curve levels off, improvements are found when the SNR becomes lower than 3.
For the orange and the volunteer the improvements are less pronounced as for the water phantom.
In signal decay curves where there is no off leveling, the SNR is larger than 3, the points are not corrected. Even the points that deviate from the straight line are not corrected. This means that the deviation is caused by another factor.

Measurement in six directions

The measurements in six directions for the water phantom are also corrected, an example of the correction is given in Figure 7.15.
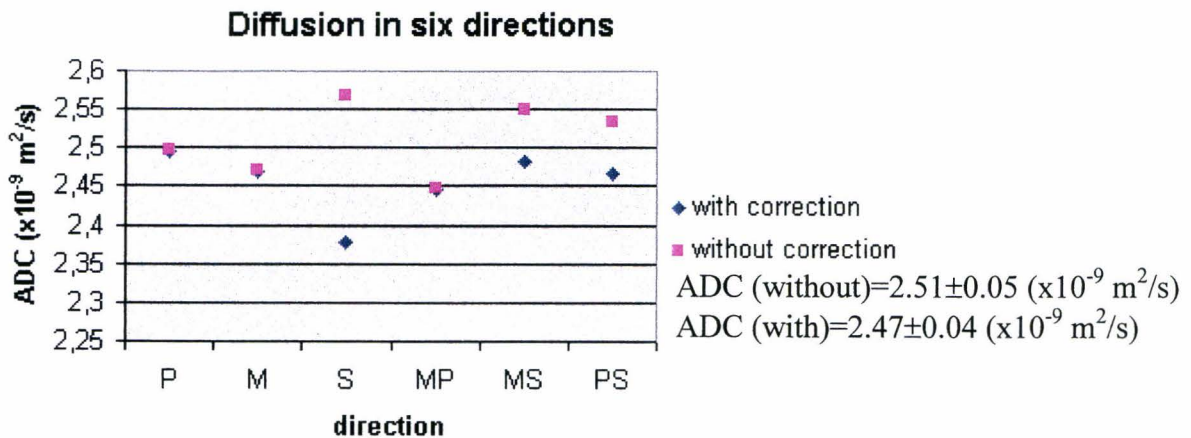

Figure 7.15: The ADC's measured in six direction before and after correction for the influence of noise.

With this correction only the average values are corrected, so nothing can be said about the SD. The average ADC for the P, M and S-direction is determined, the difference in the averages is 11.48%. For the correction this difference was 18.44%, the results are improved. When all ADC's measured are compared using the different protocols the difference found is 24%, which is the same as before correction.

Gaussian distribution

Based on the results in [10] it is assumed that the noise of the clinical system used in this study is Gaussian distributed.
A measurement is performed to check this, the results are given in Figure 7.16.
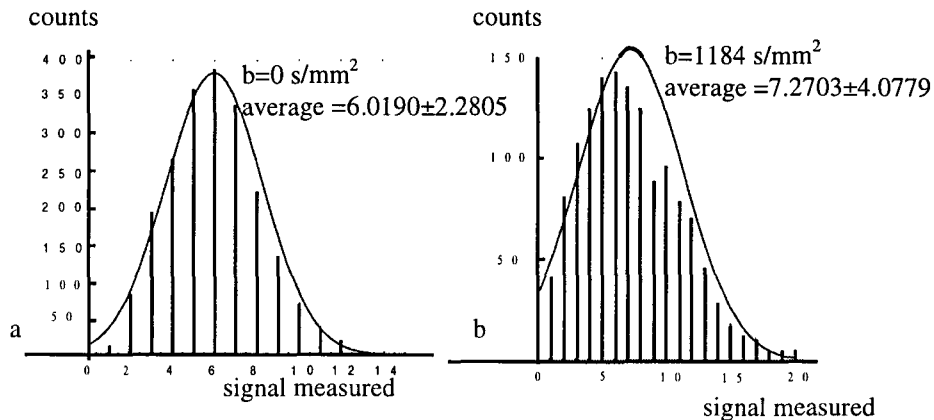
Figure 7.16: Noise distribution for an image measured a without PFG's b) with PFG's, b=1184 s/mm². The curves are the Gaussian distributions for the measurements.

The noise appears to be Gaussian distributed when no PFG's are on during the measurements. When the PFG's are on the histogram and the curve of the Gaussian distribution seem to be shifted relative to one another.

Discussion

The correction method proposed by [10] corrects only when the SNR is lower than 3. The SNR becomes only lower than 3 when the signal decay curve levels off. When the SNR comes close to 1, no correction is possible anymore.
The average ADC of the P, M and S direction is improved.
Noise has an influence on the ADC's, but only for SNR lower than 3 a correction is useful. From the correction it can be concluded that the off leveling of the signal decay curves in our setup is caused by noise and not by the difference between the diffusion of intra- and extra–cellular water.
It is assumed that the noise is Gaussian distributed, but when PFG's are used this is not the case. The effect that this has on the correction method should be further examined.

Chapter 8
Conclusions and recommendations.

The aim of this study was to examine whether the DWI can be used for the early detection of hypoxic ischemia and whether the ADC is accurate enough to be used quantitatively to classify the phase of an infarct and the brain development.
In this chapter the conclusions of this study are given first, followed by recommendations.

§8.1 Conclusions

Hypoxic ischemia and brain development

The ADC measured for ischemic tissue is decreased by 40-50% compared to the ADC's for healthy tissue. The attenuation is large enough to distinguish the ischemic from the healthy tissue, making it possible to use the ADC for the early detection of hypoxic ischemia.

The inter human variation in the ADC measured for the volunteers is small. Because the variation is small the ADC can possibly be used to measure the neonatal brain development. This will be further examined in the next coming years.

The question if the ADC can be used to classify the phase of an infarct can not be answered, because the group of newborns suffering from hypoxic ischemia from which ADC's are obtained is too small.

Accuracy of the ADC

From the measurements in chapter 4 it could be concluded that the ADC depends on the used maximum b-value. More measurements are performed to examine whether the ADC is also accurate enough to be used quantitatively.
From the results of these measurements it can be concluded that the ADC depends on the parameters that are used. When scans are made using different parameters, the ADC's cannot be compared quantitatively, but as long as the scans are made on the same scanner using the same parameters then they can be compared. The correction methods did not improve the quantitative ADC significantly.

§8.2 Recommendations

Protocols

Because the ADC can be compared when the same parameters are used, it is recommended to use the same protocol for all the diffusion scans.

New software (release 8) is installed on the MR scanner, resulting in a change of the protocols that are used for DWI. How the ADC is influenced by this needs to be checked first, before the ADC's measured using the new software, are compared to the 'normal values' in appendix B.

Number of b-values

To limit the scan-time for the comfort of the patients, especially for the newborns suffering from hypoxic ischemia, the use of three b-values is recommended above two b-values. The ADC found with 3 b-values is more reliable than found with 2 b-values and the scan-time is acceptable.
At this moment b=0, 400 and 800s/mm^2 are used in the protocol for the newborns. When a measurement is performed using b=0 and 400 s/mm^2, a large standard deviation is found within a region of interest. Maybe the use of other b-values can improve the results, but for higher b-values the SNR can be a problem.

ROI

Often a ROI contains more than one tissue, resulting in an over- or underestimated ADC. Maybe a maximum acceptable standard deviation within an ROI can be defined for an ADC to be accepted or rejected. Furthermore is it important to give a standard deviation (SD) to each ADC, because a large SD can be an indication that more than one tissue is inside the ROI.

The range of b-values for which the SD within a ROI is below 5% depends on the parameters that are used. Measurements to check this can give a better inside in which b-values should be used.

DTI

Because the quantitative use of the ADC value is limited, DTI might provide extra information about brain development and structure in ischemic regions. DTI can also be used to visualize the brain development. To determine the direction of the diffusion, the eigen-values of the ADC's measured in six directions must be calculated. The errors in the eigen-value and eigen-vector caused by the inaccuracy of the ADC should be closer examined. The way that the tissue structure is visualized should also be taken in consideration, [14] [15] [16.].

References

[1]   Vlaardingerbroek M.T, Boer den J.A. Magnetic Resonance Imaging. Springer-Verlag,1999

[2]   Potchen E.J, Haacke E.M, Siebert J.E, Gottschalk A. Magnetic Resonance Angiography, concepts and applications.Mosby ,1993

[3]   Hashemi R.H, Bradley jr. W.G. MRI the basics. Williams &Wilkins,1997

[4]   Hornak P.J. The Basics of MRI.

[5]   Boer,den J.A, Folkers P.J.M. (Philips). MR perfusion and diffusion imaging in ischaemic brain disease. MR Clinical Science, Philips Medical Systems, Best, The netherlands, 1998

[6]   Nicolaij K, Diffusion Weighted Imaging. A course in vivo NMR. Oct. 2000, wageningen

[7]   Simpson J.H, Carr H.Y. Diffusion and Nuclear Spin Relaxation in Water. Physical Review 1958; vol 111,No 5, 1201-1202

[8]   Conturo T.E, McKinstry R.C, Aronovitz J.A, Neil J.J. Diffusion MRI:Precision, Accuracy and Flow Effects. NMR Biomed 1995;8:307-332

[9]   Matiello J, Basser P.J, Le Bihan D. The b matrix in Diffusion Tensor Echo-Planar Imaging. MRM 1997;37:292-300

[10]   Dietrich O, Heiland S, Sartor K. Noise Correction for the Exact Determination of Apparant Diffusion Coefficients at low SNR. MRM 2001;45:448-453

[11]   Mulkern R.V, Gudbjartsson H, Westin GF, Zengingonul H.P, Gartner W, Guttmann C.R.G, Robertson R.L, Kyriakos W, Schwartz R, Holtzman D, Jolesz F.A, Maier S.E. Multi-component apparant diffusion coefficients in the human brain. MRM 2000;44:292-300

[12]   Clark C.A, Le Bihan D. Water diffusion Compartmentation and Anisotropy at High b values in the human brain. MRM 2000;44:852-859

[13]   Huppi P.S, Murphy B, Maier S.E, Zientara G.P, Inder T.E, Barnes P.D, Kikinis R, Jolesz F.A, Volpe J.J. Microstructural Brain Development After Perinatal Cerebral White Matter Injury Assessed by Diffusion Tensor Magnetic Resonance Imaging. Pediatrics Mar 2001;Vol.107 No.3:455-460

[14]   Shimony J.S, McKinstry R.C, Akbudak E, Aronovitz J.A, Snyder A.Z, Lori N.F, Cull T.S, Conturo T.E. Quantitative Diffusion-Tensorr Anisotropy Barin MR Imaging: Normative Human Data Analysis. Radiology 1999;212:770-784

[15]   Basser P.J, Pajevic S. Statistical Artifacts in Diffusion Tensor Imaging MRI (DT-MRI)Caused By Background Noise. MRM 2000;44:41-50

[16]   Armitage P.A, Bastin M.E. Utilizing the Diffusion-to-Noise Ratio to Optimize Magnetic Resonance Diffusion Tensor Acquisition Strategies for improving Measurements of Diffusion Anisotropy. MRM 2001;45:1056-1065

Acknowledgements

Appendix A

Scan parameters

☐ *DWI Newborns*
▨ *DWI Volunteers*

Geometry					
Coil selection	head	head	Chunks		
connection	default	default	Stacks	1	1
			type	par	par
FOV (mm)	150	230	slice	18	18
RFOV (%)	75	75	slice thickness	4.0	6
Foldover suppression	No	No	orientation	TRA	TRA
			foldover direction	RL	RL
Matrix scan	128	128	slice gap (mm)	default	user defined
Matrix reconstruction	256	256			1.0
Scan percentage (%)	80	80	Slice scan order	default	default

contrast					
Scan mode	MS	MS	Diffusion Mode	SE	SE
Scan technique	SE	SE	TE	80	80
Modified SE	No	No	Nr of b	3	4
Fast Imaging mode	EPI	EPI	order	desc	desc
EPI factor	13	13	Max b	800	1200
TSE factor			direction	PMS	PMS
Gradient mode	default	default			
SAR mode	default	default			
TE (first) (ms)	26	22			
Flip angle (deg)	90	90			
TR	4 beats	2 beats			

motion		
Cardiac synchronisation	trig	trig
Cardiac device	ppu	ppu
Cardiac frequency	130	70
Cardiac R-R window (%)	10,10	10,10

Appendix B

In this appendix the complete tables with normal values are given for the healthy volunteers (Table B.1), the healthy newborns (Table B.2), and the tables for newborns suffering for hypoxic ischemia are given (Table B.3 and Table B.4).

Healthy Volunteers

Volunteer	GM anterior (x10^{-9} m^2/s)	GM posterior (x10^{-9} m^2/s)	WM anterior (x10^{-9} m^2/s)	WM posterior (x10^{-9} m^2/s)	CSF (x10^{-9} m^2/s)
1	0,86±0,05	0,86±0,05	0,74±0,06	0,72±0,09	3,36±0,19
2	0,82±0,06	0,81±0,07	0,76±0,10	0,75±0,13	3,83±0,56
3	0,85±0,07	0,82±0,05	0,61±0,08	0,69±0,07	3,30±0,32
4	0,88±0,07	0,87±0,05	0,78±0,08	0,76±0,07	3,39±0,22
5	0,85±0,07	0,84±0,05	0,72±0,08	0,76±0,07	3,28±0,51
6	0,87±0,06	0,83±0,04	0,74±0,06	0,68±0,04	3,09±0,18
7	0,85±0,07	0,84±0,05	0,78±0,08	0,74±0,08	3,02±0,46
8	0,81±0,05	0,82±0,05	0,71±0,08	0,74±0,07	3,82±0,27
9	0,80±0,11	0,85±0,03	0,75±0,13	0,79±0,06	3,59±0,24
10	0,83±0,08	0,83±0,06	0,79±0,05	0,73±0,05	3,27±0,17
11	0,80±0,08	0,85±0,07	0,76±0,07	0,75±0,08	3,56±0,40

Table B.1: Normal values found for the healthy volunteers, volunteers 1-7 are men, 8-11 are women.

Healthy Newborns

Healthy newborn	Basal ganglia (x10^{-9} m^2/s)	WM Anterior (x10^{-9} m^2/s)	WM Posterior (x10^{-9} m^2/s)	CSF (x10^{-9} m^2/s)
1	0,73	1,04	1,04	2,41
2	0,67	1,20	1,13	2,54
3	0,83	0,91	0,98	2,13
4	0,79	1,07	0,97	2,57

Table B.2: Normal values found for the healthy newborns.

The ADC is determined at the position of the infarct, and if possible in the same tissue on the contra-lateral side, the results are listed in Table B.3. When the ADC's are determined contra-lateral the same ROI is used as for the ischemic tissue.

The ADC is also determined at the same locations as by the healthy newborns, these ADC's are listed in Table B.4. When this location coincides with the location of ischemic tissue, then no value is given. By newborns 1 and 2 only two b-values (b=0, 400 s/mm^2) are used by the other newborns three b-values are used (b=0, 400, 800 s/mm^2).

Newborn	Position of the infarct	Number of b-values	Ischemic ADC (x10^{-9} m^2/s)	Contra-lateral (x10^{-9} m^2/s)
1	WM	2	0,29±0,04	0,79±0,10
2	WM	2	0,49±0,05	0,68±0,04
3	WM	3	0,45±0,10	0,88±0,13
4	WM	3	0,29±0,04	0,49±0,08
5	Basal Ganglia (GM)	3	0,55±0,05	0,88±0,06
6	WM	3	0,71±0,06	1,10±0,04
7	WM	3	0,44±0,06	0,73±0,04
8	Basal Ganglia (GM)	3	0,49±0,04	1,13±0,07

Table B.3: ADC's measured in ischemic tissue and in the same tissue contra-lateral.

Newborn	Basal Ganglia (x10^{-9} m^2/s)		White matter, anterior (x10^{-9} m^2/s)		White matter, posterior (x10^{-9} m^2/s)		CSF (x10^{-9} m^2/s)
	Right	Left	Right	Left	Right	Left	
1	0,55±0,06	0,64±0,03	0,80±0,05		0,64±0,04		1,53±0,16
2	0,63±0,04	0,64±0,03	0,93±0,05	0,91±0,05	0,85±0,04	0,77±0,04	1,32±0,11
3		0,76±0,05		0,86±0,07		0,61±0,06	2,74±0,33
4	0,71±0,06	0,70±0,05	0,99±0,13	0,92±0,11	0,73±0,08	0,72±0,05	2,50±0,41
5	0,70±0,04	0,60±0,07	0,74±0,08	0,75±0,07	0,76±0,05		2,03±0,09
6	0,64±0,07	0,67±0,07	1,01±0,08	1,06±0,07	0,99±0,06	0,85±0,07	2,04±0,21
7	0,79±0,03	0,82±0,05	1,00±0,07	0,88±0,07	1,14±0,04	1,13±0,05	1,90±0,17
8	0,66±0,10	0,73±0,09	0,99±0,08	1,02±0,12	0,96±0,12		2,37±0,38

Table B.4: ADC's measured at the same positions as by the healthy newborns.

Appendix C

In Table C.1 the ADC's found for the water phantom, the orange and the volunteer when the gradient strength (G) is varied for different TE_{diff} are listed.

TE_{diff}	b_{max}	Water phantom ADC $(\times 10^{-9} m^2/s)$	r^2	Orange ADC $(\times 10^{-9} m^2/s)$	r^2	Volunteer ADC $(\times 10^{-9} m^2/s)$	r^2
150	6400	1,80	0,987	1,33	0,984	0,67	0,973
150	3200	1,70	0,974	1,54	0,979		
150	1600	1,90	0,986	1,87	0,979		
150	1200	2,10	0,994	1,77	0,980		
150	800	2,20	0,997	1,85	0,963		
150	400	2,30	0,998	2,21	0,986		
125	3200	1,90	0,993	0,84	0,978		
125	2400	1,70	0,970	0,97	0,985		
125	1600	2,00	0,986	1,13	0,990		
125	800	2,20	0,997	1,34	0,976		
100	1600	2,00	0,999	1,11	0,994		
100	1200	2,10	0,997	1,20	0,990		
100	800	2,20	0,996	1,37	0,977		
100	400	2,40	0,994	1,70	0,970		
75	700	2,20	0,996	1,33	0,988		
75	600	2,30	0,995	1,42	0,989		
75	500	2,40	0,995	1,56	0,990		
75	400	2,60	0,995	1,72	0,982		
75	300	2,70	0,995	1,81	0,975		
75	200	3,00	0,996	2,08	0,978		
75	100	3,30	0,998	2,57	0,964		

Table C.1: ADC's found for the water phantom, the orange and the volunteer.